STRUCTURAL STUDIES ON CARBON MATERIALS

FOR ADVANCED SPACE TECHNOLOGY

National Aeronautics and Space Administration

Research Grant Number NGR 48-002-129

NASA Technical Officer: Dennis Discus, Materials Division
NASA-Langley Research Center

FINAL REPORT

(Total Grant Period, 15 September 1971 - 31 May 1974)

Part I. Structure and Oxidation Behavior of Some Carbon/Carbon Composite Materials

D. B. Fischbach, Principal Investigator

D. R. Uptegrove, Research Assistant

S. Srinivasagopalan, Research Assistant

UNIVERSITY OF WASHINGTON

College of Engineering

Department of Mining, Metallurgical and Ceramic Engineering
Roberts Hall, FB-10
Seattle, Washington 98195

31 May 1974

PREFACE

Among elemental materials in common engineering use, carbons and graphites are notable for the wide range of properties available. This can be ascribed to a strong structure-sensitivity which has its basis in the anisotropic bonding and crystal structure, and is greatly enhanced by the broad range of microstructures which result from the many ways in which synthetic carbons may be prepared. This research project was undertaken with the broad objective of contributing to the understanding of the important and complex inter-relation of microstructure and properties of carbon materials that are useful in aerospace applications. From the start, the term microstructure has been interpreted in its broadest sense, for it was recognized that morphology and structural features at all size scales, from the atomic level thru apparent crystallite dimensions to the size, shape and arrangement of the component phases (including voids) of composite carbons are important. However, particular interest was directed toward application of scanning electron microscopy (SEM), with its great depth of field and extensive zoom magnification range (20 to ≥ 20,000 x) to a study of a few selected carbon materials. SEM observations were supplemented with other techniques such as optical microscopy, x-ray diffraction, density and porosity measurements, etc. wherever necessary or advantageous.

The capabilities of the SEM are especially well suited to the observation of irregular surfaces; the planar, polished surfaces required for high magnification optical study are neither necessary nor especially desireable. The greatest benefit from SEM studies therefore appeared to lie in the observation of natural surfaces, especially those generated by processes with important applications significance. Two particular areas, oxidation and fracture, were singled out initially for study. Attention was focused primarily on three general categories of carbon materials: "Massive" pyrolytic carbons which are dense, graphitic and strongly anisotropic; glass-like carbons which are microporous and impermeable, non-graphitizing and largely isotropic; and a class of anisotropic carbon/carbon composities of carbon fiber cloth laminated with a carbon binder phase. (Carbitex^{R} materials from the Carborundum Company.) Both cleavage and "tensile" (three point bending) fracture surfaces were studied to characterize the microstructure and deduce information about fracture behavior of as-deposited and annealed pyrolytic carbons, and of "graphitized" Carbitex materials. Observations were also made on bending fracture surfaces of several grades of glassy carbon. Results of these studies were presented and discussed in previous progress reports [1 - 3]. In the later stages of this project, these observations on macroscopic fracture behavior led to an interest in the localized deformation and fracture processes in microhardness indentation. These indentation studies were necessarily limited to homogeneous carbons (mostly glass-like carbons, and some pyrolytic carbons). Some initial results were reported earlier [3], and our further studies in this area form the topic for one half of this final progress report. In a similar way, the oxidation behavior of glass-like, pyrolytic and composite carbons was initially surveyed [2,3], but interest was finally focused on the behavior of the Carbitex composites. Three

different grades of material, differing in heat treatment history, were studied, and considerable attention was paid to characterization of the microstructures as well as to the oxidation behavior of these composites. The results of these studies form the topic of the other half of the final progress report.

The final report on this research grant, then, consists of two parts. Each is essentially a summary and interpretation by the principal investigator of the major content of a thesis submitted in partial fulfillment of the requirements for the Masters Degree in Ceramic Engineering. Part I, "Structure and Oxidation Behavior of Some Carbon/Carbon Composite Materials," represents the work of David R. Uptegrove; Part II, "Indentation Hardness Behavior of Some Homogeneous Carbons," contains the work of Seshadri Srinivasagopalan. Ultimately, both theses will be on file in the Engineering Library of the University of Washington, and photocopies will be obtainable thru the usual channels. Papers on both of these research projects were presented at technical meetings [4, 5, 6]. It is a pleasure to thank A. Miller and M. Rorabaugh for assistance on x-ray diffraction; and C. S. Kucheria for help with the porosity and surface area measurements. The principal investigator also received important primary support under NASA Grant NGR 48-002-004.

SUMMARY

I. Structure and Oxidation Behavior of Some Carbon/Carbon Composite Materials

The microstructure and some microstructural effects of oxidation have been investigated for the following Carborundum Company Carbitex laminar carbon fiber cloth/carbon binder matrix composite materials: C-100 (carbonized fiber and binder); C-500 (graphitized fiber, carbonized binder); and C-700, C-730 (two different cloth weaves of graphitized fiber in graphitized binder). Although only these particular materials were studied, many of the characteristics observed are thought to be relevant to carbon fiber/carbon binder composites in general.

Cloth weave is important in determining the macrostructure of the composites. C-100, 500, 700 were constructed of a plain weave cloth and appeared less anisotropic than C-730 which was made from a flatter satin or twill type weave. X-ray diffraction analysis showed that in general the composites were more graphitic (lower mean interlayer spacing) than their constituent fiber phases, indicating a graphitic binder matrix phase. C-700, 730 were well graphitized with definite (100)/(101) modulation. A significant binder layer-plane orientation texture (parallel to fiber axes) was observed in all the composites. Bulk and immersion (benzene/tetrabromoethane) densities indicated that C-100 was binder-poor, and that accessible porosity increased in the order C-500 (7.4%), C-730, C-100, C-700 ($\lesssim$13.5%). Mercury intrusion and CCl_4 adsorption porosimetry combined with BET surface area measurements showed that in general the pore distribution is trimodal and occurs primarily in the entrance-diameter range >200 A (C-500 also had a small amount of open porosity in the range <200 A). The principal pore size modes include macropores (mean diameter $\geq$100 μm), apparently at unimpregnated weave interstices, etc.; medium diameter pores (2.5 to 7 μm depending on composite grade) due primarily to gaps between plys or yarns; and small pores ($\approx$0.45 μm) associated with the binder/fiber interface and the binder matrix. The detailed pore size distribution of the composites depends on both the cloth weave and the thermal treatment history. Fiber porosity appeared to be negligible. High pressure mercury porosimetry caused irreversible structural damage to the composites. SEM observation of polished cross section surfaces identified the major pore modes, and revealed that two binder phases are present: A laminar, oriented primary binder and a more isotropic impregnant binder. Examination of cleavage surfaces showed that the fibers are coated with thin binder films which are wrinkled but adherent in C-700, 730, and unwrinkled but less adherent in C-100. Fiber/binder bonding in C-500 is very poor relative to that in the other composites.

The quantitative oxidation behavior was determined by measuring sample weight loss as a function of time at 650°C in flowing dried air using a modified thermogravimetric apparatus. The burnoff rate decreased in the order C-100, 500, 700, 730. Oxidation rates of C-700, 730 were about an order of magnitude lower than those of C-100, 500. Initially, rates increased with time, then decreased at high burnoff levels (>30% weight loss). These results are very similar (except for absolute rates) to data obtained earlier at 550°C in ambient air, which also showed that the oxidation rates of glassy and pyrolytic carbons were about an order of magnitude lower than that of C-730. The small reactivity differences between C-700 and C-730 and between C-100 and C-500 correlate qualitatively with porosity differences, but fiber graphitization in C-500 and binder deficiency in C-100 also contribute in the latter pair. The large reactivity difference between C-100, 500 and C-700, 730 must be attributed primarily to the influence of graphitization treatment on purity and/or structural disorder, especially of the binder phase.

Sequential SEM observations were made on selected areas of cleavage and polished section surfaces as a function of oxidation weight loss. In general, the lateral surfaces of the fibers were attacked first, especially at the bottoms of the longitudinal surface grooves characteristic of rayon-based fibers. The fiber cores are less reactive and remain after extensive burnoff. In C-100, after the initial stages of oxidation, the carbonized binder and fibers phases appear to be consumed at about the same rate. The average reactivity of the fiber phase is decreased by graphitization in C-500, and at high burnoff levels appears to be less than that of the carbonized binder. However, a strong heterogeneous attack occurs on bare graphitized fibers at active sites distributed randomly along their lengths. For both C-100 and C-500, sample volume tended to decrease in rough proportion to weight loss at high burnoff levels, due perhaps to falloff of unburned material loosened by the oxidation attack. Thus a part of the high reactivity observed for these materials may be apparent rather than real. For C-700, 730 macroscopic sample size and shape changed little even at high burnoff levels. Graphitization of the binder phase reduces the oxidation rate in these composites in two ways: The graphitized binder is significantly less reactive than the fibers; and the adherent binder film coating the fibers tend to protect them from attack.

These results show that, under the moderate temperature and oxidant flow conditions studied, C-700, 730 exhibit superior oxidation resistance primarily because of the inhibiting influence of the graphitized binder matrix. However, the rate of attack is still high compared with that of glassy and pyrolytic carbons and could perhaps be further reduced by more effective binder impregnation. Without considerable densification (and perhaps purification) of the composite, long-term oxidation resistance is likely to be poor. However, short-term resistance could probably be improved significantly if the external surfaces were thoroughly sealed by graphitized binder. Therefore, it is recommended that exposed surfaces be used in the as-fabricated condition whenever possible. If the composite must be machined, a final surface impregnation and graphitization bake might improve performance. A pyrolytically deposited coating might also be effective.

I. STRUCTURE AND OXIDATION BEHAVIOR OF SOME CARBON/CARBON COMPOSITE MATERIALS

D. B. Fischbach and D. R. Uptegrove

Introduction:

The term carbon/carbon composite generally connotes materials composed of carbon fibers in a carbon binder matrix. Although the use of fibrous carbons as the major filler phase is relatively new, these materials actually belong to the same category as the ordinary and familiar synthetic electrographites. The property levels and anisotropy of such composites depend strongly upon the nature of the dominant filler phase. The use of fibrous carbons makes possible much higher property levels, but also generally greatly increases the anisotropy of the composite. Actually, both the macroscopic anisotropy and the performance capabilities depend upon a number of factors including the amount and arrangement of the fibers (unaxial tows, plys or yarns; biaxial laminates of various cloth weaves, etc.); the nature of the binder matrix and binder/fiber interactions; and the details of the fabrication and processing as well as the characteristics of the fibers.

The particular composites studied here are members of the family of Carbitex® materials produced by the Carborundum Company. They consist of carbon-fiber cloth laminates impregnated with a carbonaceous binder and subsequently carbonized and, in some cases, given a high temperature graphitization treatment. Three different grades of materials, differing in heat treatment history, were investigated: C-100 carbonized fiber cloth in a carbonized binder matrix; C-500, "graphitized" fiber cloth in a carbonized binder matrix; and C-7X0, "graphitized" fiber cloth in a graphitized binder matrix. Two subclasses of the last category, C-700 and C-730, differ in the cloth weave used. C-700 and C-500 are constructed of GSGC-2 cloth, a simple "square" over one/under one plain weave of two-ply yarn with a "unit cell" comprising a 2x2 yarn rectangle measuring about 2 x 2.2 mm. The same weave, ungraphitized, is used in the C-100 material. The GSGC-8 cloth weave used in C-730 is a twill or satin type weave, of single ply yarns in a complex over one/under seven pattern with the "over" positions of adjacent yarns offset by three yarns. The "unit cell" is an 8 x 8 yarn square measuring about 4.5 mm on a side and the texture is denser and flatter than that of the GSGC-2 weave. These two weaves were illustrated and the effect of weave on composite properties was discussed in a previous report [1]. Nominal property data for the 100, 500 and 700 composites, published by the manufacturer [7], is given in Table I.

TABLE I

Some Properties of Carbitex Materials According to the Manufacuturer[6]

Property \ Grade	100	500	700
Density, g/cm^3	1.38	1.40	1.44
Flexural Strength, 10^3psi	14	17.6	11
Compressive Strength, 10^3psi			
With Grain	8	10.2	7.6
Against Grain	45	40	21
Young's Modulus, with grain, 10^6psi	1.6	2.7	1.3
Coefficient of Thermal Expansion, $10^{-3}/°C$			
With Grain	1.6	1.1	1.05
Against Grain	1.5	2.5	3.3
Electrical Resistivity, 10^{-3} ohm-inch			
With Grain	0.25	0.20	0.06
Against Grain	5.5	0.35	0.17
Purity (%Elemental Carbon)	99.5	99.7	99.9

The objective of this investigation was to study the microstructural aspects of oxidation attack on these composites, and the influence of the different thermal histories and cloth constructions on the oxidation behavior. The general procedure used was SEM examination of selected areas of cleavage or polished cross-section surfaces as a function of increasing oxidation attack at a single temperature. Weight-loss vs time curves at this temperature were determined in a separate set of measurements on samples similar to those used for the SEM studies. In order to interpret these observations, it was necessary to characterize the nature and microstructure of the composites as completely as possible. Unfortunately, very little information could be obtained from the manufacutuer regarding the precursor materials or processing details. A considerable supplementary effort was therefore made to determine the nature of these composites in somewhat more detail. Some features could be inferred from microstructural observations; others were deduced from various diagnostic and property measurements that were carried out to help characterize the materials. These are discussed in the following section. Succeeding sections of the report deal with the experimental prodedures used in studying the oxidation behavior, the characteristic features observed, and their interpretation.

Characterization of Carbitex Materials:

The carbon-fiber cloth was presumed to have been prepared by carbonization of a textile fiber cloth. The irregular cross-sectional shapes of the fibers are characteristic of materials prepared from rayon textile precursors. Mean fiber diameters are in the range 8-10 μm. Since development of high mechanical property levels in such fibers requires stress carbonization or stress graphitization processing which are not appropriate for woven cloth, the fibers were expected to have low preferred orientation texture, and only moderate strength and elastic modulus ($\leq 10 \times 10^6$ psi). Strong supporting evidence for these suppositions was provided by diamagnetic susceptibility and density measurements reported earlier [3], and by x-ray diffraction measurements to be described below. Observations on both interlaminar cleavage and polished cross section surfaces indicated that successive cloth layers were stacked in alternating 0, 45, 90 and perhaps 135 degree aximuthal orientations (relative to warp/woof directions in the weave). The binder-impregnated cloth layers were evidently subjected to compression normal to the layers during carbonization (and/or during curing if a thermosetting resin binder was used), as evidenced by the high density of layer packing, the appearance of the cleavage surfaces, and the flattened shape of binder-impregnated yarns visible in polished cross sections (on in fragments extracted from fractured samples) as well as by statements in the manufacturer's brochures. Although some indirect evidence suggested that the binder was of the thermoplastic type (e.g., coal tar pitch), no definitive information was obtained on this point and it is possible that a thermosetting binder such as furfuryl alcohol resin was employed. Micrographic studies to be described later strongly suggested that the composites had received at

least one binder impregnation treatment after the initial carbonization bake. If either pre- or post-impregnation treatments were used, there is the further possibility that more than one type of binder material was used in fabricating the composites. Optical and SEM observations showed that, in general, binder impregnation of individual yarns was good, but porosity between plys in the yarn, between yarns in the cloth weave, and between layers in the composite appeared to be fairly common and extensive. Density and porosimetry measurements, described below, confirmed the presence of extensive (7-14%) open porosity distributed among several fairly well-defined pore entrance-size ranges. In terms of the ability of the composites to mark paper, of their qualitative fracture behavior, and their response to specimen preparation operations such as sawing, grinding and polishing, the carbonized C-100 and C-500 materials were definitely much "harder", more brittle and more abrasive than the "graphitized" 700 and 730 materials. Since graphitized cloth was necessarily used in making the C-500 composite, it was presumed that the C-700 and C-730 materials were also constructed of graphitized cloth, and the composite was given a further post-carbonization heat treatment to graphitize the binder. In that case, the fiber phase in the 700 and 730 materials might differ somewhat from the fibers in the 500 material because of the additional heat treatment and perhaps the influence of constraints on the fiber phase in the composite during treatment.

X-Ray Diffraction:

Rough x-ray diffraction spectra were run on all of the composite materials to obtain information on the degree of graphitization. A sample of GSGC-2 cloth, as well as powdered (200 mesh) samples of C-100, C-500, C-700, C-730, GSCY-2-10 carbon fiber yarn, yarn from GSGC-2 cloth, and SP-1C graphite (Union Carbide Corp.) were run on a Norelco diffractometer with Ni-filtered Cu Kα radiation. Profiles of the (002) layer plane diffraction peak are compared in Fig. 1. The SP-1C graphite (002) peak occurred at the same position with about the same half-width as the C-700, 730 peaks but was too intense to be plotted on the scale shown and has therefore been omitted from the figure. Diffraction spectra in the 2θ range 36 to 60°, which include the (10) and (004) peaks, are shown in Fig. 2. All of these spectra were taken with the same instrument settings, and no corrections have been made for background, Geiger tube counting losses, etc. The patterns have been displaced arbitrarily along the ordinate for display and comparison purposes, but approximate zero levels are indicated along the right edge of the plots.

No clear resolution of contributions from the fiber and binder phases was observed in any of the diffraction patterns, but comparison of the spectra of the various materials did yield some interesting qualitative information. From Fig. 1 it can be seen that the (002) peaks for the C-100 composite and the GSCY carbon fiber occur at relatively low angle and are weak and broad, characteristic of very disordered carbons. Furthermore, the patterns for the composite and for the fiber alone are very similar, although the materials are too disordered for subtle differences to be distinguished. For the graphitized GSGC cloth and the C-500 composite the peak is stronger, narrower, and shifted to higher angle (lower d_{002}), and has a distinctive

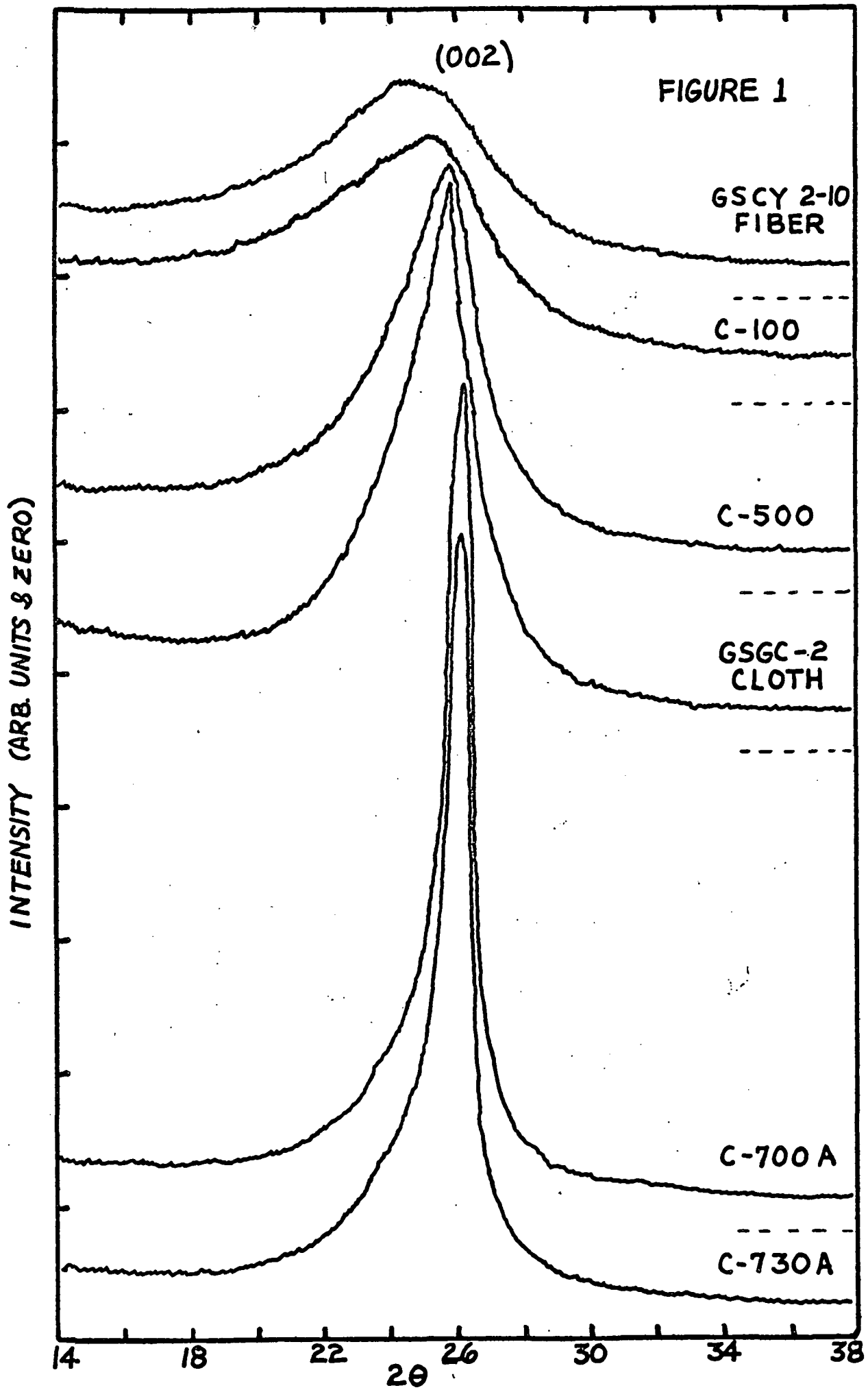
(002)
FIGURE 1
GSCY 2-10
FIBER
C-100
C-500
GSGC-2
CLOTH
C-700 A
C-730 A
INTENSITY (ARB. UNITS & ZERO)
14
18
22
26
30
34
38
2θ

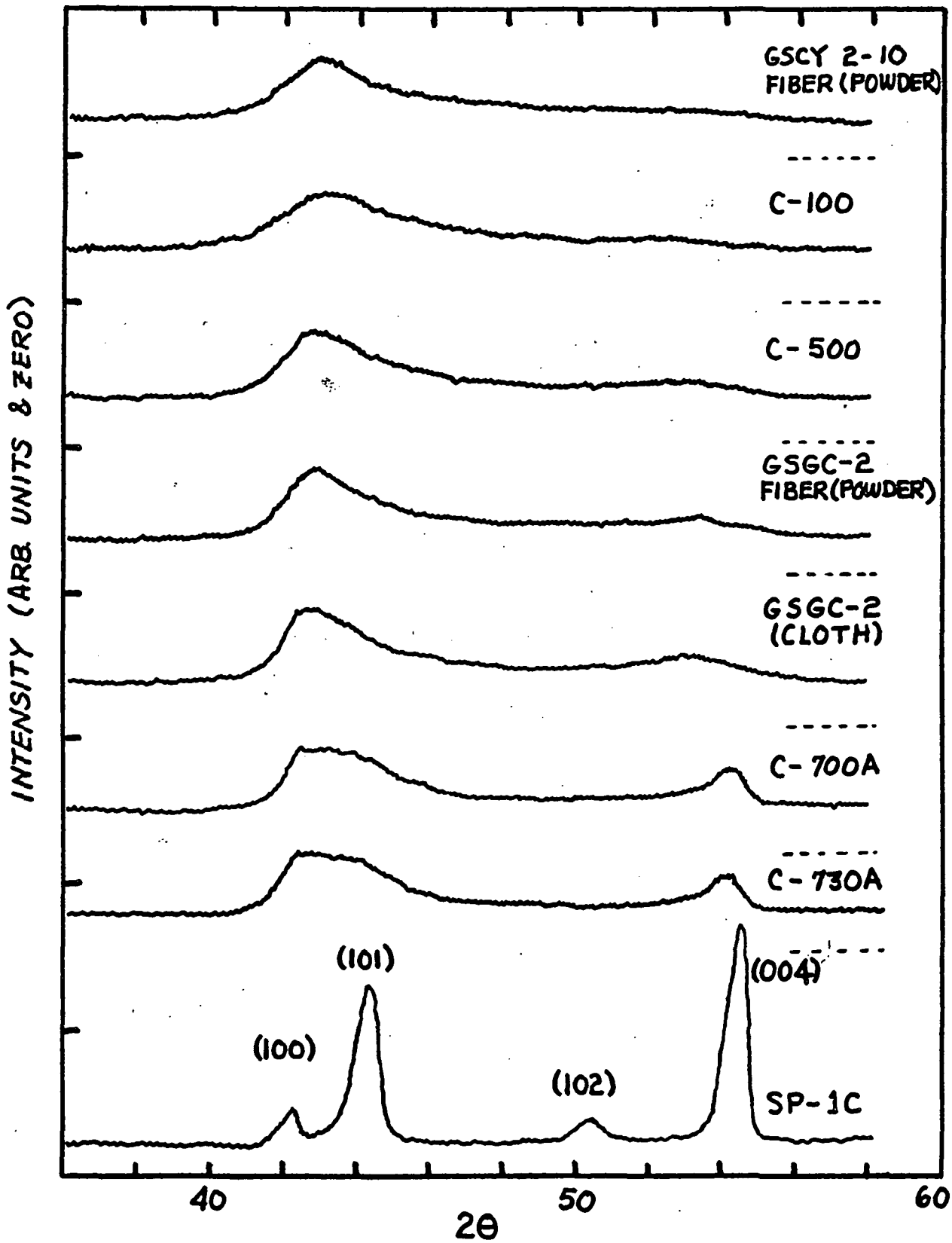

Figure 2. X-ray diffraction profiles in the (10) - (004) peak range. Conditions same as for Fig. 1: Dashed lines indicate zero levels; all samples powdered except GSGC-2 cloth.

sharply-peaked assymmetrical shape. The (002) peaks for the C-500 and the powdered GSGC fiber (not shown) were identical within experimental uncertainty. The very close similarity of patterns for these carbonized composites and for the binder-free samples of the fibers used to make them is interesting. It suggests that the fiber phase completely dominates the diffraction response (because it is dominant in composition, and/or because the binder pattern is very weak and diffuse compared with the fiber pattern so that it doesn't contribute much). The patterns for the graphitized C-700, 730 are also very similar to each other, but differ greatly from that of the free fiber phase in being much sharper and shifted to higher angle. This suggests that the graphitized binder phase now dominates the diffraction behavior, (but the low angle tail on the composite (002) peaks is similar to that observed for the free fiber phase). Similar conclusions follow from examination of the (10) and (004) diffraction peaks shown in Fig. 2. The two-dimensional order (10) peak, which is quite broad for the GSCY fiber and the C-100 composite, seems a little sharper in the GSGC fiber and the C-500 composite, but there is no indication of modulation into (100) and (101) peaks (indicative of developing layer stacking order) in any of these materials. However, a very definite (101) bulge has developed on the high-angle side of the (10) peaks in the C-700, 730 graphitized composites. This could result from superposition of a well-graphitized binder pattern on the more disordered pattern from the fibers. A parallel development occurs in the (004) peak, which cannot be resolved in GSCY fiber or C-100 composite patterns; is weak and broad but detectable in the GSGC fiber and C-500 composite patterns; and is quite well developed in the C-700, 730 composites. However, the development of these features is far short of that exhibited by the well ordered SP-1C graphite, and even the graphitized composites contain appreciable structural disorder (presumeably largely in the fiber phase).

In order to obtain some information about possible preferred orientation textures, as well as to check on the diffractometer observations, Debye-Scherrer films were run in a small (57 mm dia.) camera for several materials. The samples used consisted of a) small bundles of parallel fibers from GSCY-2-10 yarn and GSGC-2, -8 cloth; and b) fragments of binder-impregnated yarn extracted from fractured pieces of C-100, 500, 700 and 730 composites. These samples were aligned with the fibers parallel to the camera axis (perpendicular to the incident x-ray beam). Only a very weak preferred orientation texture was evident in the patterns for the bare fibers. This result is consistent with previous observations made here on several varieties of low modulus carbon fibers made from pitch or rayon. However, in all cases, the binder-impregnated yarn fragments extracted from the composites exhibited a definite layer-plane fiber texture (most pronounced in the C-730 sample). This texture evidently results from an oriented binder phase. In the graphitized composites texture was evident in the (006) and (008) lines which are not visible in the bare fiber patterns and therefore evidently originate from the binder. Although there appear to be no mechanisms by which the observed textures could have been generated in the fiber phase of the composites, there are plausible mechanisms for the appearance of such texture in the binder matrix. Carbonization of

thermoplastic binder materials like pitch occurs by the formation of an anisotropic liquid mesophase which agglomerates and loses hydrogen to form the final coke residue. This mesophase nucleates and grows preferentially on solid surfaces exposed to the pitch, and is oriented with the mesophase layer planes parallel to the substrate surface[8]. Through this process, one would anticipate that a highly oriented film of binder carbon would form on the fiber surfaces wetted by the binder pitch, though the orientation texture might decrease in the interstices between the fibers. Direct SEM observations of laminated binder films around the fibers will be shown later. A similar texture can develop in thermosetting binders due to constraint, by the solid filler phase, of binder shrinkage during carbonization[9]. This deformation process also converts the binder into a graphitizable carbon; but the considerable stresses developed may destroy fiber/binder adhesion and even damage or fracture the fibers and/or the matrix[10]. This makes unlikely the use of thermosetting resins for the primary binder matrix.

Quantitative results obtained from the XRD analyses are summarized in Table II. Values obtained from the Debye-Scherrer films are reported directly, while values measured from the diffractometer patterns are enclosed in parentheses. The approximate values for L_a, the apparent layer plane diameter, were obtained from the displacement of the (10) peak intensity positions from the graphite value (rather than from peak width).

TABLE II

X-Ray Diffraction Results on Carbitex Materials

Material / Parameter, A	$d_{(002)}$	$d_{(004)}$	$d_{(006)}$	$d_{(008)}$	$La_{(10)}$
GSCY-2-10 fiber	3.49	3.48	-	-	~30
	(3.60)	-	-	-	(~50)
C-100	3.52	3.43	-	-	-
	(3.51)	(3.46)	-	-	-
GSGC-2, 8 fiber	3.43	3.426	3.421	-	~67
	(3.45)	(3.435)	-	-	(~76)
C-500	3.42	3.385	-	-	-
	(3.45)	(3.44)	-	-	-
C-700	3.345	3.363	3.364	3.362	~90
	(3.39)	(3.38)	-	-	-
C-730	3.371	3.356	3.356	3.360	~114
	(3.40)	(3.39)	-	-	-
SP-1C	-	3.35	3.35	3.352	-
	(3.39)	(3.367)	-	-	-

The interlayer spacing values determined from the diffractometer traces are consistently higher than the values determined from the Debye-Scherrer films, probably indicative of some diffractometer misalignment since film shrinkage was negligible in all cases. The degree of graphitization indicated by the $d_{(00\ell)}$ values increases regularly in the order listed in the table, from GSCY carbon fiber to the C-700/730 graphitized composites and the SP-1C graphite powder. The composites consistently appear more graphitic than the fiber phases they contain (based on the Debye-Scherrer $d_{(004)}$ values). The most reasonable interpretation of these XRD results is that the more graphitic phase dominates the diffraction behavior (strong narrow peaks dominate coincident broad weak peaks), and the binder carbon is consistently more graphitic than the fiber phase. This conclusion would be consistent with the use of a high-quality thermoplastic binder. However, appreciable layer stacking disorder persists even in the graphitized binder phase (no clear resolution of 100 and 101, although 110 and 112 are well-developed in the graphitized composites).

Density:

Bulk (apparent) densities of all the composites were determined on the large blocks (30 to 40 cm^3) as received from the manufacturer, and on smaller rectangular prism specimens (about 1 cm^3) cut from these blocks. Immersion densities of the GSGC-2,8 and GSCY-2-10 fibers as well as of small samples of the composites were determined in a benzene-tetrabromoethane (B/T) density gradient column calibrated with glass-bead standard floats at intervals of about 0.1 g/cm^3. For the final immersion density measurements, samples were evacuated with a mechanical pump and impregnated with a B/T solution of approximately the expected density. After introduction of the samples into the column, readings were taken over a period of several days to insure that they had settled to their equilibrium buoyancy levels, and to allow the fluid within the pores to equilibrate with the column fluid. In general, vacuum impregnation made little difference in the results when the samples were small and long equilibration times were allowed.

The average bulk and immersion density results are summarized in Table III, along with the nominal bulk density values published by the manufacturer. Bulk densities of our samples differed somewhat from the nominal values; there were significant differences between different blocks of the same grade of materials; and in some cases there were differences among samples cut from the same block. These differences can probably be ascribed primarily to processing variations (especially the effectiveness of laminar compaction and binder impregnation), but measurement errors may have contributed as well. The immersion densities also varied somewhat from sample to sample and from lot to lot. Reliable densities are particularly difficult to obtain for the fibers because there is often a significant distribution of density values, individual fibers tend to become entangled with each other, and the fibers settle to equilibrium positions very slowly. The density of the carbonized GSCY fibers appears to be slightly less than that of the GSCG-2,8 fibers which have generally similar

TABLE III

Average Density Values for Carbitex Materials

Material	Value	Nominal ρ_β, g/cm^3 (Table I)	Bulk Density ρ_β, g/cc	Immersion Density ρ_l, g/cc	Vol. Fraction of Pores $(1-\rho_\beta/\rho_l)$%	Specific Pore Vol. $(1/\rho_\beta - 1/\rho_l)$ cm^3/g
GSCY-2-10 fiber		-	-	1.458	-	-
GSGC-2 fiber		-	-	1.480	-	-
GSGC-8 fiber		-	-	1.480	-	-
C-100		1.38	1.327	1.474	10.1	0.076
C-500		1.40	1.439	1.552	7.4	0.051
C-700A		1.44	1.427	1.624	12.3	0.086
	B		1.416	1.637	13.5	0.095
	C		1.446	1.668	13.3	0.092
C-730A		1.44	1.468	1.623	9.7	0.068
	B		1.468	1.606	8.6	0.058

values. Sample-to-sample and block-to-block variations in the immersion densities of the composites may result in part from experimental error (residual gas bubbles trapped in small pores; small-sample deviations from the average composition; etc.), and in part from real variations in the fiber/binder ratio from block to block and from point to point within a block. The density of the binder phase is not known, but is evidently appreciably higher than that of the fibers, as evidenced by the density values for C-500, 700 and 730. Since the density of the C-100 composite is only slightly larger than the fiber density, our sample of this material must either contain an unusually small fraction of binder, or more closed porosity than the other composite grades.

The true significance of the immersion densities measured here is somewhat uncertain. The values obtained depend, of course, on the extent to which the immersion fluid fills the pore volume of the material. This in turn depends upon the size and entrance diameter of the pores, the effective molecular diameter of the fluid, and its ability to wet the pore surfaces. The most generally accepted method for obtaining the "true" density is helium picnometry, but unfortunately the facilities for this type of measurement are not currently available here. It has been reported[11]

that very nearly the same density values are obtained for nuclear-grade synthetic graphite by both helium and benzene methods; but for certain chars with small pore-entrance diameters the helium density is appreciably greater than the benzene density. If the amount of small-entrance-diameter porosity is negligible, the immersion densities measured here should provide a valid indication of the open porosity. Porosimetry and surface area measurements discussed in the next section indicate that this is the case for the Carbitex materials. Pore volumes (both per cm^3 and per g of sample) calculated from the observed bulk and immersion densities are also listed in Table III. On this basis open porosity increases in the order C-500, 730, 100 and 700.

Porosimetry:

More detailed information about the amount and size distribution of accessible porosity was obtained by the technique of mercury porosimetry. The pore size distribution can be calculated from the volume of mercury intruded into a sample as a function of applied pressure since the pressure P required to force mercury into a pore is inversely proportional to the entrance diameter D of the pore (and a function of surface tension of the mercury γ and the wetting angle θ): $D = 4\gamma\cos\theta/P = 175/P$ where D is in μm, P in psi, γ = 474 ergs/cm^2, θ =130°. (According to [12] a better value of the constant for graphite is 213; this would increase the indicated pore sizes by 22%.) Large pores are filled at very low pressures and are very difficult to measure by this method. The present data corresponds to pore volumes associated with entrance diameters smaller than about 100 μm.

Cummulative pore volume (cm^3/g of sample) is plotted as a function of mercury pressure and the corresponding pore-entrance diameters for the free fiber phase and the C-100 and C-500 composites in Fig. 3 and for the C-700 and C-730 composites in Fig. 4. The porosimetry behavior of the carbon fiber cloth used for making the composites was measured in an attempt to establish a "base-line" for comparison. Fabrics of this sort contain a very large void volume and it was necessary to divide the results by a factor of 5 to 10 to fit them onto the same scale as the composites. The data shown in Fig. 3 are for GSGC-2 cloth (x 1/5), but qualitatively similar results were also obtained for GSGC-8 cloth and GSCY-2-10 yarn. Most of the pore volume in these materials consists of the interstices between fibers in the yarns and between yarns in the weave, but much of the porosity in the vicinity of the knee of the curve (in the range 0.5 to 2 μm) may be attributable to the longitudinal surface grooves characteristic of fibers made from rayon. There is virtually no accessible porosity below about 0.5 μm in any of the free fiber materials. Impregnation with binder and fabrication into a laminar composite, of course, substantially affects the amount and distribution of the porosity. Total pore volume is greatly reduced in the composites, and a trimodal distribution of pore sizes developes. Although the mercury data gives little more than a hint of the presence of pores with diameters greater than 100 μm, microstructural observations as well as density data (in combination with the porosimetry and surface area results discussed here) indicate that there is a significant volume of such large pores in the Carbitex composites. In the carbonized C-100 and 500

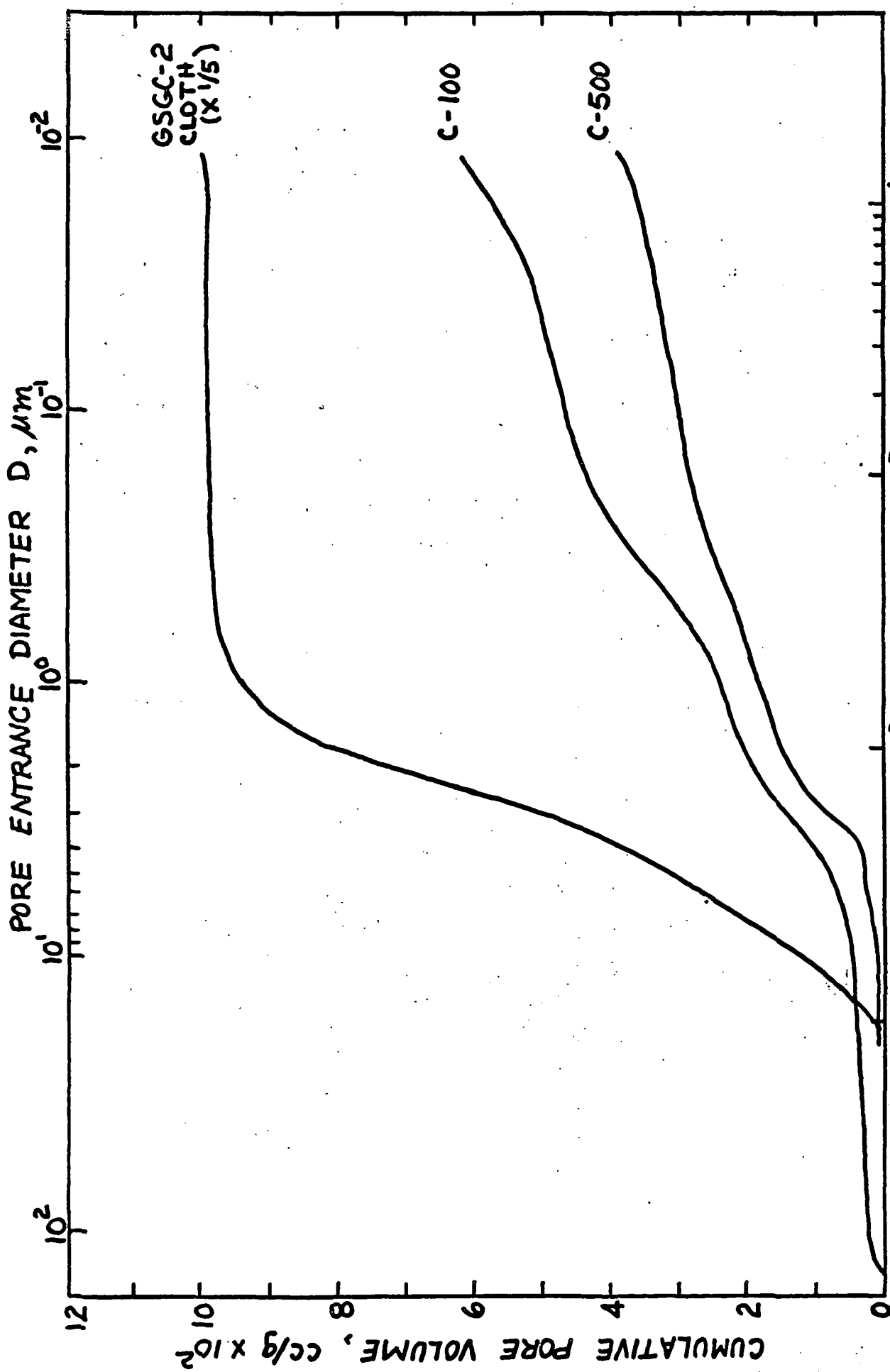

Figure 3. Mercury porosimetry results on "graphite" fiber cloth and on carbonized-matrix composites.

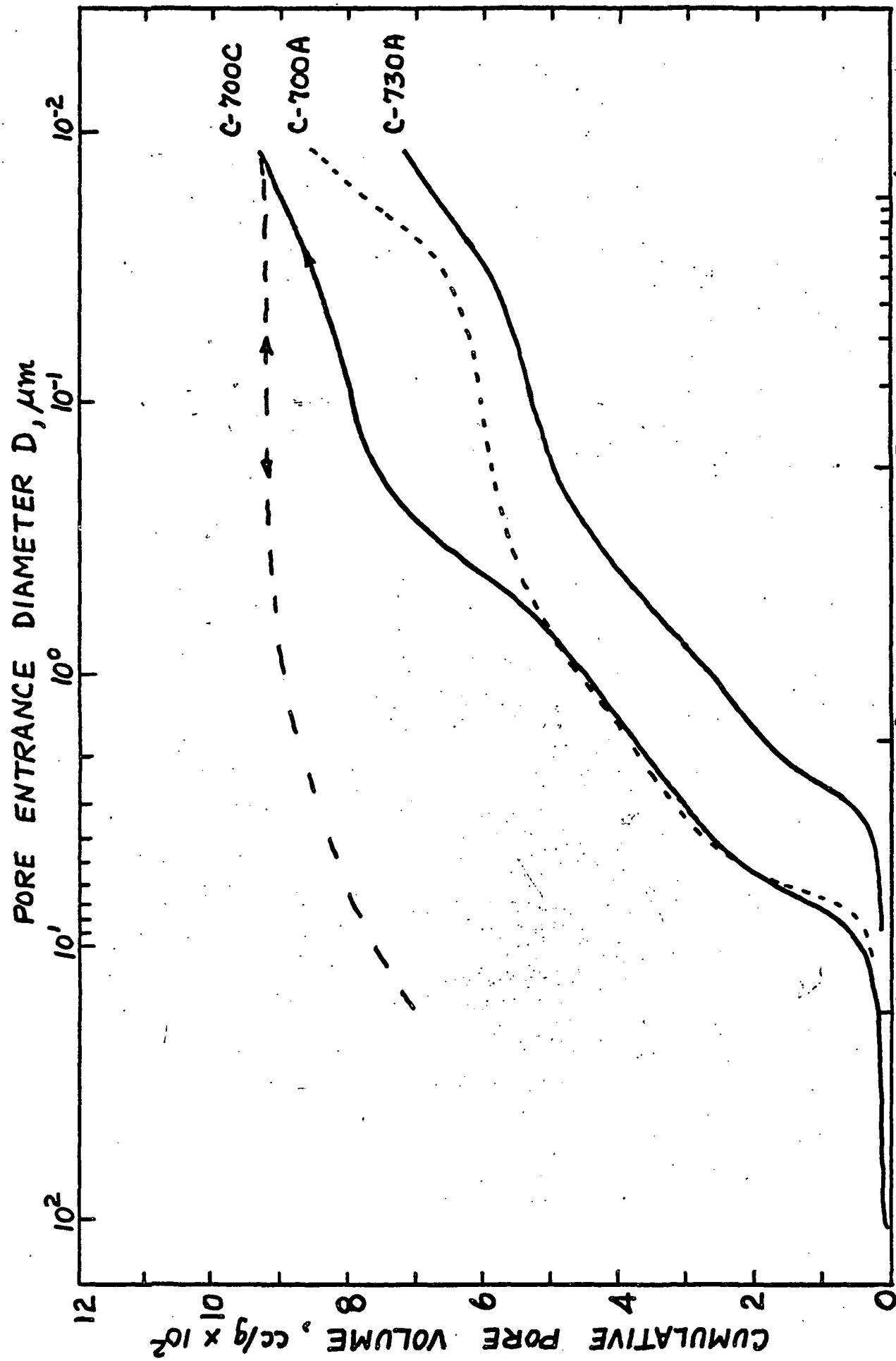

Figure 4. Mercury porosimetry results on graphitized composites.

composites a sharp rise in pore volume occurring around a mean pore diameter of about 3.5 μm, is tentatively attributed to incomplete binder penetration between yarns in the cloth, or perhaps between cloth layers. A second rise, more clearly defined in C-100 than in 500, which occurs in the vicinity of 0.45 μm pore diameter, is tentatively attributed to incomplete filling of the surface crennulations of the fibers by the binder, to voids between the fibers in the yarns, and/or to cracks between the fibers and binder. With the possible exception of C-500, the further rise in apparent pore volume in the high pressure range corresponding to pore diameters less than about 0.06 μm appears to be largely an artifact, as will be discussed below. The relatively large pore volume in C-100 (in comparison with that in C-500) correlates well with the low density of this composite and seems consistent with the hypothesis of binder deficiency.

The pore distributions of the graphitized C-700 and C-730 composites are also trimodal and the pore volumes are significantly larger, as shown in Fig. 4. The C-700 would be expected to be similar to C-500 in all respects except thermal history. The graphitization treatment has shifted the average diameter of the medium-sized pore mode upward by a factor of two to about 7 μm, and the total pore volume is greater by a factor of 2 to 3 than in the C-500. This can be attributed to the combined effects of anisotropic shrinkage of the oriented binder as a result of graphitization (the mean interlayer spacing decreases by more than 2%), and of cracks caused by differential thermal expansion stresses generated on cooling from the treatment temperature. The solid curve is representative of data obtained on samples from two different blocks (700 B,C); but a third block (700A) had a substantially lower accessible porosity in the small pore region, as indicated by the dashed line. For C-730, the distribution of pores is qualitatively similar to that in C-700, but the average medium-range pore size is smaller (about 2.5 μm) and the total pore volume is less. Nearly identical results were obtained on samples from two different blocks (730 A,B). This change in pore distribution seems quite consistent with the flatter, denser fabric weave (GSGC-8) in these composites which might be expected to reduce the size and frequency of voids between cloth layers and in weave interstices.

The continued increase in apparent pore volume in the high pressure range corresponding to pore entrance diameters less than about 0.06 μm (especially evident for 700 and 730) is unexpected and so an attempt was made to determine whether this represents a true component of the pore distribution, or simply an artifact of the measurement method. A large pore volume in this small size range would generate an appreciable surface area (unless pores are of the ink-bottle type with internal diameters much larger than entrance diameters). Therefore, BET type (nitrogen adsorption) surface areas were determined for C-100, 500 and 700C with an Aminco Sor BET apparatus and compared with the surface area estimated from the observed pore distribution assuming a cylindrical pore geometry. Although the estimated surface areas for C-100 and 700C were in excess of 3 m^2/g, the BET results indicated that the actual values were less than

1 m^2/g (below the measurement range of the apparatus). However, for C-500 a value of 3.6 m^2/g was measured, compared to an estimated area of $\geq$1.9 m^2/g. As a further test, the total volume of pores with diameters <0.02 μm in C-100, 500, 700A, 700C, 730B and <0.2 μm in C-500, 700A, 730B was determined by a method involving condensation of CCl_4 vapor in the pores. Again, negligible porosity in these small pore ranges was indicated for all samples except C-500. For this material values of about 0.006 cm^3/g were obtained for both measurements indicating that the additional porosity occured only in the smallest size range. This result is in approximate quantitative agreement with the BET measurement. Two conclusions follow from these results: a) C-500 contains a small but significant amount of microporosity beyond the range of the mercury intrusion measurements, and b) the large apparent pore volumes in the range D <0.06 μm indicated by mercury porosimetry for the other materials are almost certainly artifacts.

Since the "mercury" pore distribution is inferred from the decrease in volume occupied by the mercury and the sample in a closed container as the applied pressure is increased, any decrease in impermeable sample volume would contribute to the apparent porosity. (Corrections for mercury and sample holder compressibility effects, determined from blank runs with no sample, were applied to the data plotted in Fig. 3, 4.) The characteristics of the high pressure data are, in fact, similar to those expected for sample compressibility effects. However, the apparent compressibilities are much larger than the published graphite value, and (more importantly) the effect is not reversible. When the pressure is released, there is a large positive hysteresis, and on repressurizing, the depressurization curve, which lies well above the initial intrusion curve, is followed approximately reversibly as shown for 700C in Fig. 4. Such hysteresis is commonly observed due to delayed and/or incomplete extrusion of mercury from the sample, and appreciable Hg was retained by the present materials as indicated by increased sample weight after testing. Nevertheless, since both BET and CCl_4 adsorption results show that there is very little open porosity in the range below about 0.1 μm in the C-100, 700 and 730 composites which show the large apparent compressibilities and hysteresis effects, it seems reasonable to assume that most of this retained Hg resides in the larger pores and should not directly cause hysteresis in the high pressure range. A plausible explanation is that permanent compaction of the samples occurred during and as a result of the mercury porosimetry measurements at high pressures.

In principle, significant changes in sample structure may be determined by repeating the porosimetry measurement after gently removing the retained Hg. This proved to be unexpectedly difficult. Moderate temperature vacuum evaporation of the retained Hg, a technique successfully applied to bone samples [13], was only partially effective. After of the order of 100 hrs at 100-166$_2$°C (Hg vapor pressure 0.27 - 5.3 torr) in a fore-pump vacuum ($\leq 3 \times 10^{-2}$ torr) weight and immersion density measurements showed that a significant amount of Hg remained in a small sample of 700A which had been intruded at about 8500 psi. Porosimetry measurements were not made because the Hg extraction was not complete, and the sample had been cut into smaller

fragments in the course of the extraction experiment, making quantitative comparison with the initial porosimetry results difficult. After this phase of the work had been completed, it was found that very similar phenomena have been reported for ordinary synthetic graphites, and have been explained in terms of the opening at high pressures of pores which are normally closed [12,14]. Much of the pore volume increase was reported to be irreversible due to rupture of pore walls, but a small fraction was attributed to irreversible elastic effects which trapped Hg as pore entrances closed on releasing the pressure. For the present materials, the entrance diameters of such "elastic" pores would evidently be < 7 A (the effective molecular diameter of CCl_4) at ambient pressure, and open to 100-500 A to admit Hg at high pressure. The phenomena occurring during high pressure Hg porosimetry of carbon materials evidently require and deserve further study. Whatever the true nature of the high pressure porosimetry phenomena, an approximate value for the normally open porosity may be obtained graphically by treating the effect as though it were due to a linear compressibility. By subtracting these corrected Hg pore volumes from the total accessible pore volumes calculated from the density data, the following volumes are obtained for the macropore (>100 μm diameter) fraction are obtained: C-100, 0.029 cc/g; C-500, 0.014 cc/g; C-700C, 0.009 cc/g; C-730A, 0.008 cc/g. The inferred accessible-pore size distributions, including the macropores, are plotted in Fig. 5 where the estimated or corrected portions are shown as dashed lines.

In summary, porosimetry and surface area measurements confirm the density data evidence of appreciable open porosity. Little if any of this porosity occurs in the pore size range 0.2 μm (2000 A) to 10 A, so the immersion-density fluid probably does penetrate most of the open porosity. The pore size distribution is trimodal with major contributions in mean entrance-diameter size ranges ≥ 100 μm, 2-7 μm and 0.3 - 0.4 μm. Both the total porosity and the detailed pore size distributions are functions of the cloth weave and processing history of the composites. Total porosities range from about 7.4 to 13.5 volume %, increasing in the order C-500, 730, 100,700. Irreversible damage to the microstructure occurs during high pressure porosimetry measurements.

Purity:

No direct assessment of sample purity was undertaken in this work. The manufacturer's literature indicates the following % elemental carbon (as shown in Table I): C-100, 99.5; C-500, 99.7; and C-700, 99.9. This progression is consistent with what would be expected from the thermal processing. Furthermore, it is stated that atomic emission spectrography on C-700 showed that the amounts of Cu, Ti, Ca, V, Al, Fe, Ni, Si and Mg are each less than 10 ppm.

Oxidation Behavior:

The oxidation behavior of the four grades of Carbitex material were examined by both macroscopic quantitative techniques and by microscopic qualitative methods. The quantitative investigation was undertaken primarily to provide a base-line for interpretation of the microscopic observations

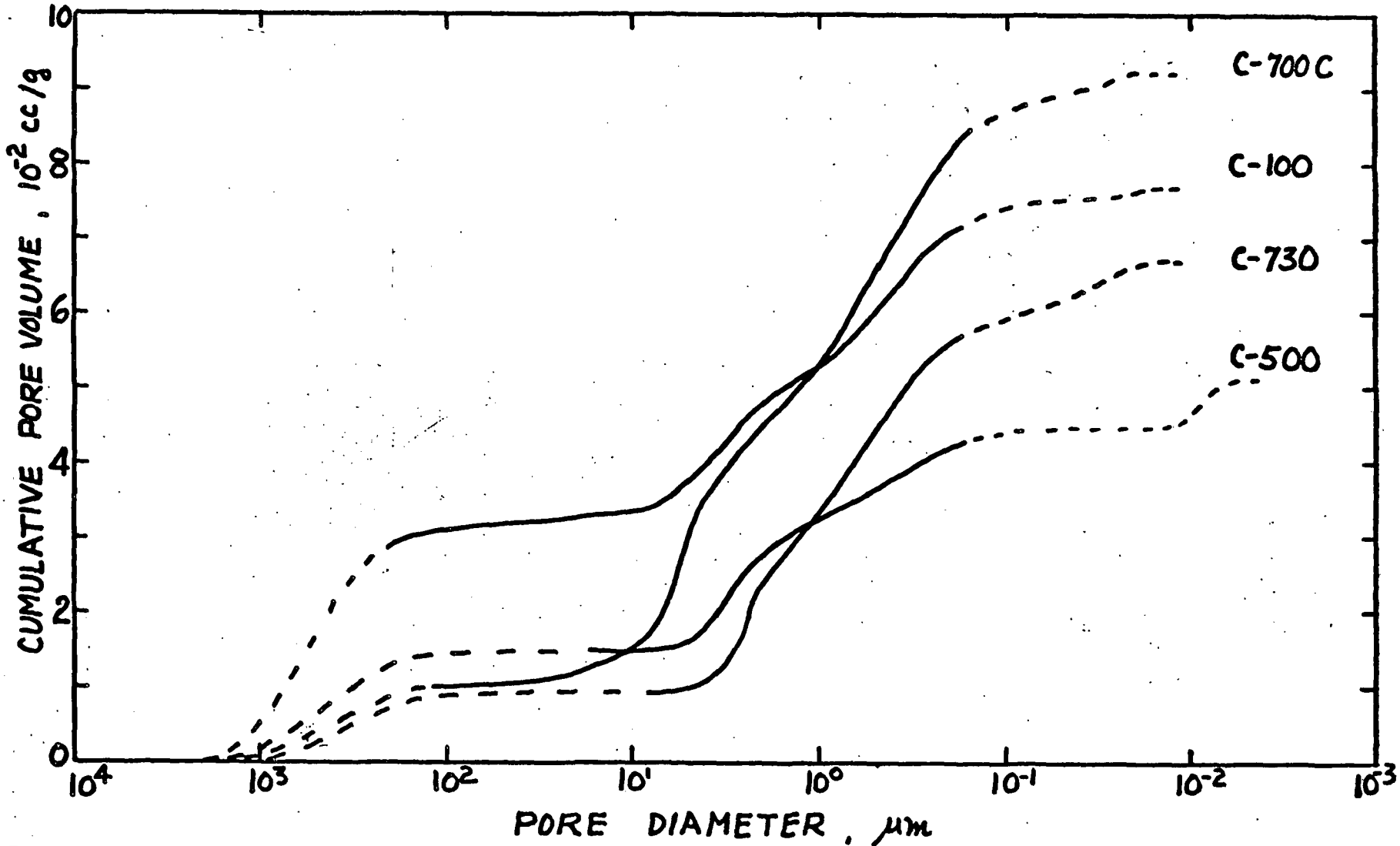

Figure 5. Total accessible pore distributions of Carbitex materials inferred from density, mercury intrusion, and CCl_4 adsorption. Solid lines, zero-adjusted Hg data; dashed lines estimated (large diameter) or corrected results (small diameter).

and was limited to determination of isothermal weight loss vs time characteristics. For both aspects of the study rectangular-prism samples (about 4x6x6 mm^3) were oxidized in air in a thermogravimetric apparatus. Laminar surfaces were cleavages and the cross sectional surfaces were polished. A single sample, contained in a platinum wire basket suspended from a single-pan analytical balance, was rapidly introduced into the at-temperature furnace and the weight loss was measured as a function of time. Continuous measurements to ≥70% burnoff were made to determine the weight loss characteristics. Oxidation of the samples for microscopic observations was done incrementally. The temperature was measured and automatically controlled using a thermocouple located immediately below the basket. Thus the temperature of the oxidizing atmosphere rather than of the sample was measured. In the initial experiments the oxidation occurred in a hindered convective flow of room air at ambient humidity. Under these conditions the burnoff vs time characteristics at 550°C were determined for a vitreous carbon (Beckwith 100°C treatment), an as-deposited pyrolytic carbon (General Electric Co., deposited at 2150°C from methane) and GSGC-2 cloth as well as of C-100, 500 and 730. These results were reported previously [3]. For the later experiments reported here the TGA apparatus was modified so that a controlled flow of clean, dried air (bottled breathing air passed through a Drierite column) was supplied to the furnace. The flow rate was adjusted to the maximum value which did not seriously distrub the balance (about 600 cc/min). This may have differed somewhat from the flow rate in the initial apparatus, but attempts to measure the convective rate were unsuccessful due to the constrictive effects of the metering apparatus.

The oxidation behavior of C-100, 500, 700 and 730 in dry air at 650°C is shown in Fig. 6. The weight loss has been normalized to unit initial external surface area (about 1.7 cm^2 for these samples), and a burnoff of 50 mg/cm^2 corresponds to loss of about one third of the initial sample weight. It is evident that the oxidation rate of the carbonized-binder composites C-100, 500 is about an order of magnitude greater than that of the graphitized C-700, 730 materials. This is in general agreement with the previous results, which also showed that C-730 oxidizes about an order of magnitude faster than does pyrolytic or vitreous carbon. The oxidation rate of the composites increases as the burnoff progresses, and there are small but characteristic and reproducible differences in the reactivities of C-100, 500 and of C-700, 730.

Material parameters which may contribute importantly to determining reactivity include purity, structural disorder and anisotropy, and accessible porosity/surface area. [15,16] In the temperature and flow regime used here oxidation is not expected to be diffusion controlled, and therefore burning should occur on internal (pore) as well as external surfaces. On this basis, the tendency for the oxidation rate to increase as burnoff proceeds may be attributed, at least in part, to increasing surface area. Micrographic observations discussed below show that pores are created and/or enlarged and surface area may also be increased by a generally heterogeneous pitting attack on exposed surfaces. The higher reactivity of C-100 relative to C-500 and of C-700 relative to C-730 correlates qualitatively with the relative porosities (cf Table III); and the very low reactivities of pyrolytic

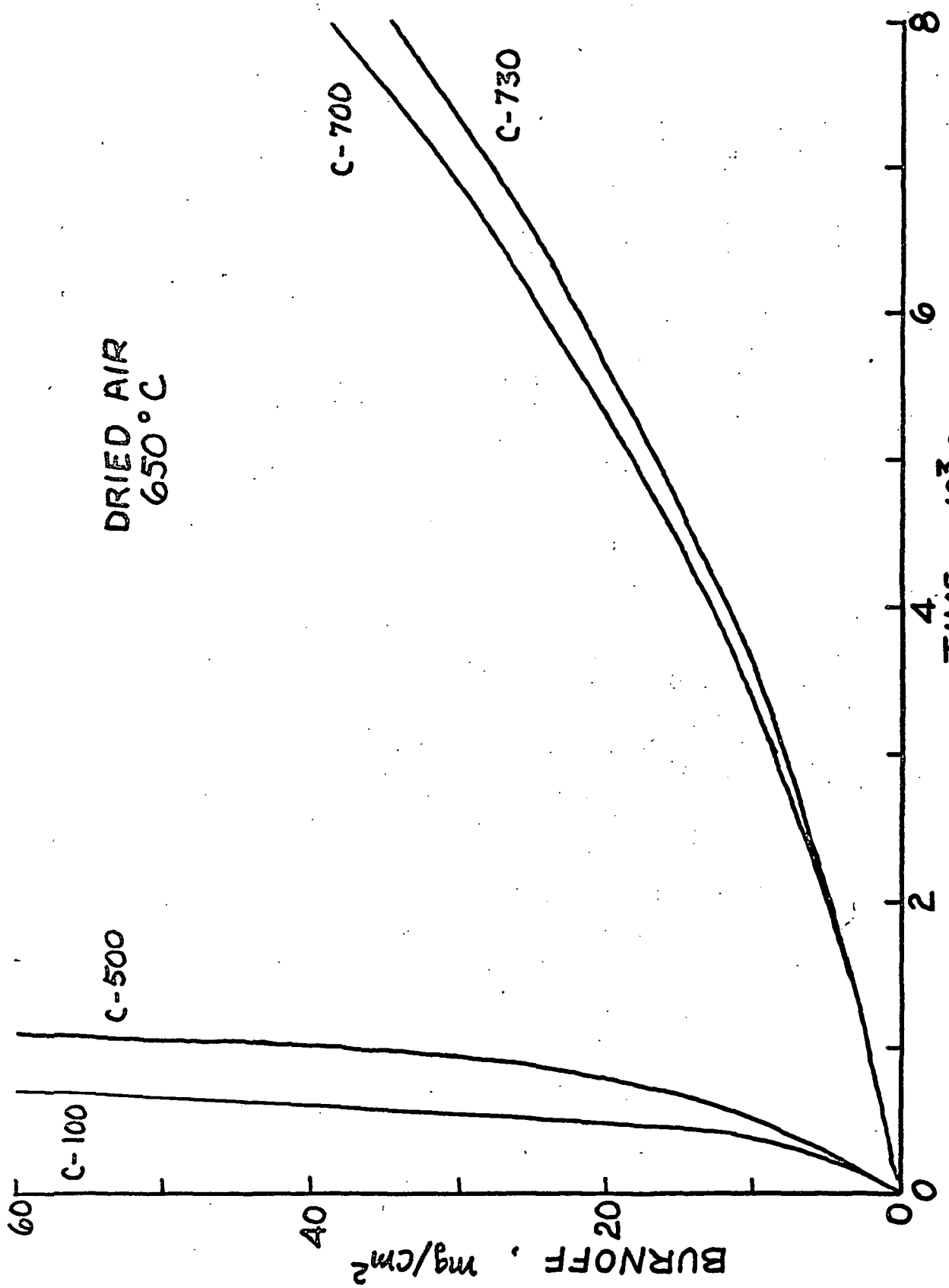

Figure 6. Isothermal weight loss (burnoff) as a function of time for representative Carbitex materials.

and vitreous carbon correlate with the negligible amounts of accessible porosity in these materials. Surface area data in hand for the Carbitex composites is not good enough for a detailed analysis of the importance of this parameter. However, it seems unlikely that porosity and surface area considerations can account for the large difference in reactivity between the carbonized and the graphitized composites. The accessible porosity of C-700 is appreciably larger than that of C-500, and the surface area of C-500 appears to be large compared with that of both C-700 and C-100. The micrographic studies suggest that microstructural characteristics (crystallographic disorder, preferred orientation texture, morphology, etc.) may contribute to the reactivity differences. The influence of microstructure on the detailed mode of the oxidation attack could be responsible for rather large effects on the weight-loss curves. It was observed that the volume of the C-700, 730 samples changed very little during burnoff, but the volume of the C-100, 500 samples tended to decrease progressively in rough proportion to the weight loss at high burnoff levels. This suggests that loss of particulate material, detached but not consumed by the oxidation attack, may contribute significantly to the weight loss and high apparent reactivity of the carbonized composites. Microstructural observations offer some support for this hypothesis. Finally, impurities may also play an important role in the observed burnoff behavior. It is well known that impurities can have a profound effect on the oxidation behavior of carbon materials. Furthermore, the thermal graphitization treatments which decrease structural disorder also significantly decrease the impurity content (by volatilization). It has also been reported [15,16] that the composition of the oxidizing atmosphere (CO_2 content, traces of H_2O vapor, etc.) may have important effects. Neither the materials nor the methods of the present study were suitable for a detailed investigation of these influences. Nevertheless, the results are considered appropriate and relevant to the behavior of real carbon materials in engineering environments.

Microstructure and the Effects of Oxidation:

The microstructures of the Carbitex composites and the effects of oxidation on them were investigated in some detail by sequential SEM observations at magnifications of from 20 to 10,000x of sample surfaces as a function of weight loss. The great depth of field and wide zoom magnification range of the SEM made it possible to relocate and examine the same microscopic regions after successive bouts of attack in the TGA apparatus. Although some general indications of the progress of the attack could be obtained at magnifications as low as 100x (field of view encompassing one or more yarns), for definitive information it was necessary to go to 1000x (a field of $\leq$ 100 fibers) to 5000x (a single fiber). This technique is capable of following the effects of the oxidative attack in great and very instructive detail; but it is also inherently very selective, and practical considerations prevent sampling a large number of regions on each sample to insure that the whole range of actual behavior is observed. However, there is a certain randomness involved in the initial selection of regions to be observed, done before the sample is subjected to any oxidation, and there was general consistency among various sets of observations which provided some reassurance that the features observed were not atypical.

Two types of surfaces, cleaved and polished, were studied. Interlaminar cleavages have the advantage of being "natural" surfaces unaffected and uncontaminated by grinding and polishing operations. The separation occurs between the cloth layers and the crack tends to propagate along the binder/fiber interface (fluctuating from one layer to the other) and sometimes transversely across the outer fibers of a ply. Such surfaces reveal quite directly the binder-impregnated cloth laminate of which the composite is made, and allow rather extensive observation of binder films, and cross sectional fracture and lateral surfaces of fibers -- but they also contain artifacts of the fracture process which may not be representative of the true internal structure of the intact composite. Cross sectional surfaces of the composites were polished by standard metallographic procedures (hand grinding on abrasive papers of progressively finer grit thru 620, followed by polishing on cloth-covered wheels thru 0.06 μm alumina in water suspension) and cleaned ultrasonically. Both longitudinal and cross sections of plys, yarns, and their constituent fibers, and the binder matrix were presented for study by these surfaces. However, these polished sections are of course quite different from the actual internal surfaces accessible to oxidation in the intact composite. There was a tendency for the fine alumina polishing grit to be embedded in and retained by the surfaces even after extensive ultrasonic cleaning (especially in the graphitized-fiber composites) but no observable catalytic effects of these particles were detected. These cross sections provided a much more representative and comprehensive view of the composite microstructure than did the cleavage surfaces. Contrast of the as-polished surfaces was generally poor, due evidently to a thin smeared film of polishing debris (probably binder carbon). This made it difficult to distinguish clearly structural details such as the boundaries between fibers and binder prior to oxidation. However, the initial oxidation attack (1 - 2 % weight loss) was an effective etchant. The pictures which follow largely speak for themselves and the commentary is provided primarily to draw attention to and interpret some particularly significant aspects. These micrographs were selected as representative examples from the much larger set of pictures obtained, and interpretations were based on the total information available. The incremental oxidations were carried out in the TGA apparatus in the hope that the microstructures could be related to the quantitative burn-off data. However, because of material losses in handling the samples (especially mounting and demounting for SEM observation), and because the oxidation attack was generally quite heterogeneous on a microscopic scale, the weight loss values on the figures are only approximate. They should be regarded as indicative of the relative amounts of exposure to the oxidation conditions rather than as quantitative measures of the observed attack.

Unoxidized cleavage and oxidized (4% weight loss) polished cross section surfaces of C-100 are shown at low magnification in Fig. 7 a,b. The general morphology is typical of all of the composites made from the plain weave GSGC-2 type cloth (i.e. C-500, 700). Large-diameter pores (or possibly pull-outs) are evident, especially at yarn intersections and weave interstices. A portion of Fig. 7b (coordinates approximately 1/3,1/3 from the lower left corner and after only 2% oxidation) is shown at higher

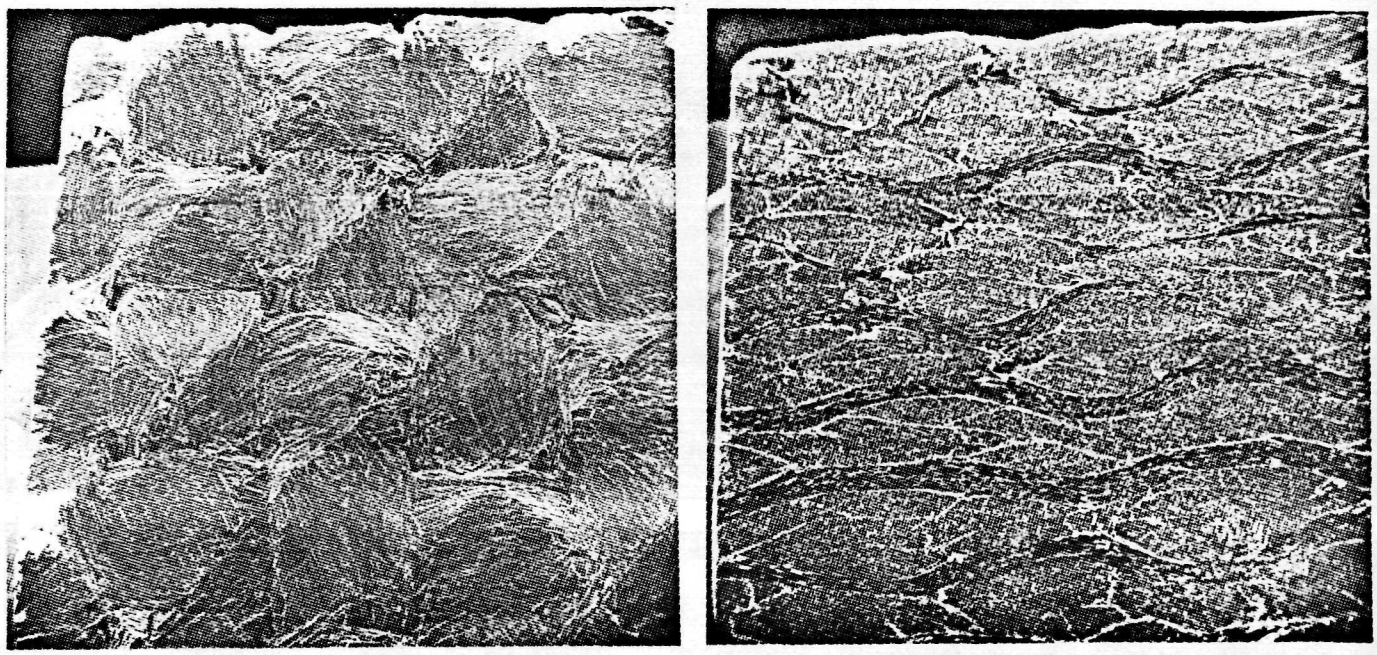

a) Cleavage, 0% burnoff, 21x. b) Polished section, 4% burnoff, 21x

Figure 7. Macrostructure of Carbitex 100.

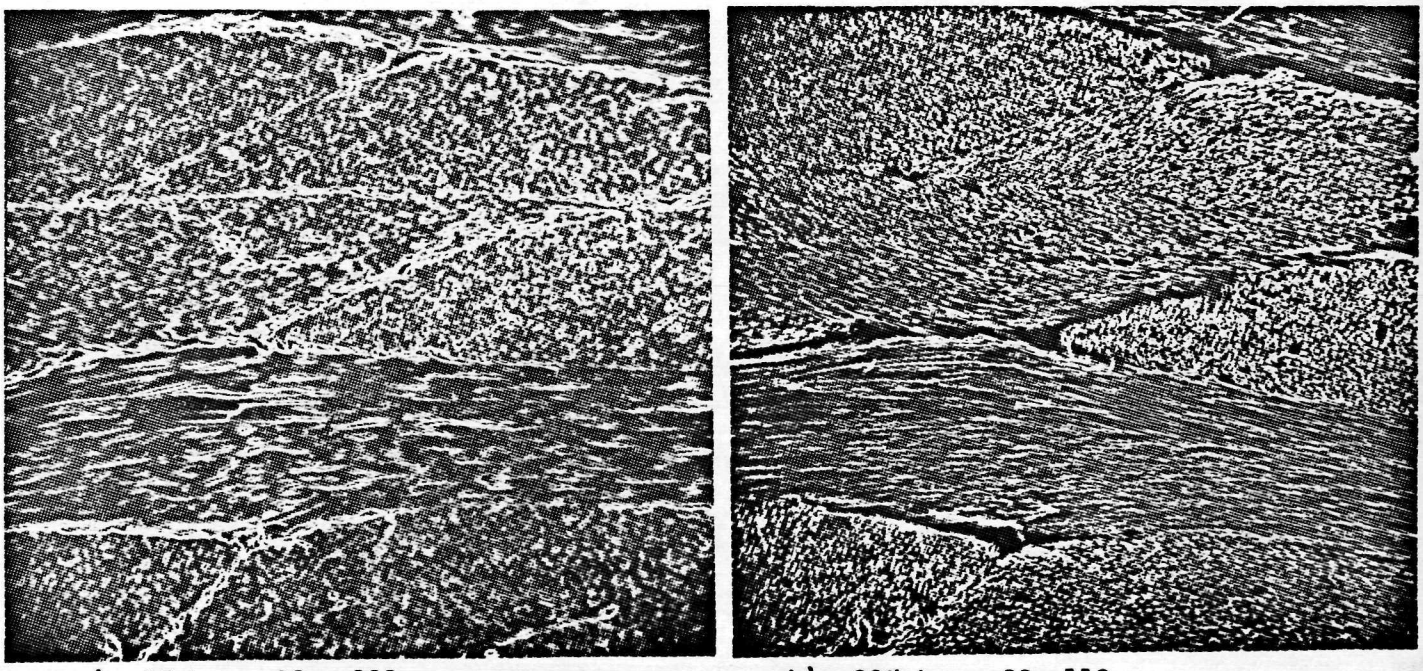

a) 2% burnoff, 111x. b) 20% burnoff, 113x.

Figure 8. C-100 polished section (detail, center of lower left quadrant of Fig. 7b).

magnification in Fig. 8 a. Considerable mid-sized porosity is evident as narrow separations between plys, yarns and/or layers and as small holes within the yarn plys. Fig. 8 b shows the same area after extensive oxidation. At this magnification it appears that the residue consists primarily of fibers, suggesting that the binder phase has been preferentially consumed. However, higher magnification studies described below show that this interpretation is not entirely correct. The separations between plys and yarns are very pronounced after oxidation, and it is evident that the field includes yarns intersecting the surface at 45 and 135 degrees as well as normally and longitudinally. The progressive development of the oxidation attack on the region in the center of Fig. 8 a,b is shown by the sequence of higher magnification views in Fig. 9 a,b,c,d. The etching effect of the initial oxidation is clearly evident in the dramatic improvement in contrast between the fiber and binder phases in going from (a) to (b). The nature of the porosity is clarified, and small-size pores are seen to have the form of thin separations within the inter-fiber binder matrix and at the fiber/binder interface. The fiber/binder ratio within the central ply is very high (consistent with the earlier inference of binder deficiency), but somewhat thicker binder films occur along the ply boundaries. Initially, the fiber phase oxidizes preferentially and two modes of attack seem to operate: There is a general burnoff of the lateral fiber surfaces that are not sealed by an adherent binder film, indicating that porosity at the fiber/binder interface plays a significant role in the oxidation behavior; and a severe heterogeneous attack, initiating as small, deep circular holes just inside the fiber periphery which increase in diameter as burnoff proceeds. Significant binder attack is not evident until fiber burnoff is well advanced, and the thicker of the binder films within the ply are still largely intact after appreciable weight loss, Fig. 9 d.

The progressive oxidation in the region of a single fiber (in a different area of the surface) is examined at still higher magnification in Fig. 10 a,b,c,d,e,f. A number of microstructural features which are obscured in the as-polished (a) sample are revealed in (b) and (c) by oxidation etching. These include transverse polishing scratches, rather clear evidence of the existence of two distinguishable binder phases (light and dark regions in the binder films), and a distinctly laminar morphology in the lighter binder phase (c,d,e). Conformation with the fiber contours and relative amounts present show that the lighter-toned material between the fibers is the initial binder. Gaps resulting from fiber separation or binder shrinkage during carbonization have been partially filled by impregnation, evidently with a different binder composition (or carbonization treatment) yielding the darker material. The laminar structures tend to confirm the inferences of binder preferred-orientation texture drawn from the X-ray diffraction observations. It is more clearly evident here (b,c) that the deep-hole oxidation attack on the fibers initiates just beneath the bottoms of some of the sharp longitudinal crennulation grooves that are characteristic of rayon-based fibers. Attack elsewhere on the fiber cross section is light and consists of shallow circular pits. The major attack on the fibers appears to occur on the lateral rather than on the cross section surfaces. Recession of the polished surface is evidently quite slow relative to the lateral attack (the deepest polishing scratch can still be discerned in d though the fiber diameter has decreased $\sim$ 2 μm), and the holes are already

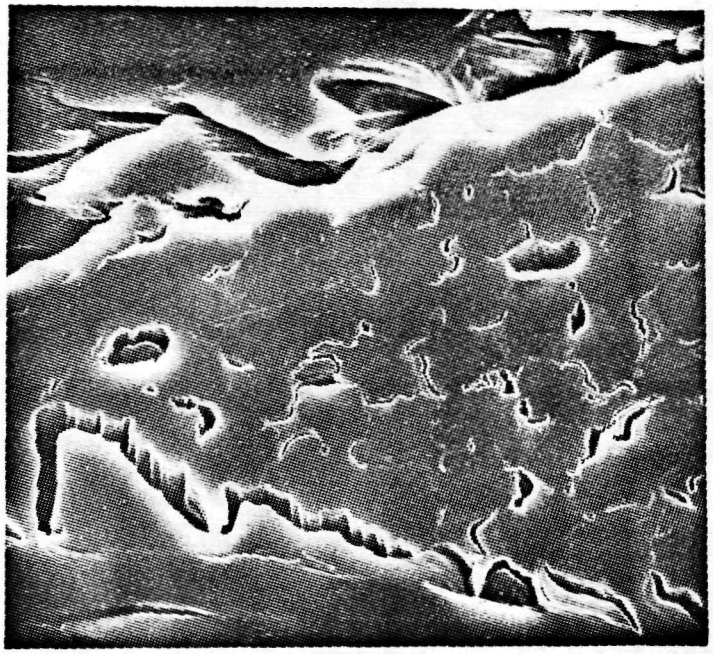

a) As polished (0% burnoff), 1068x.

b) 4% burnoff, 1072x.

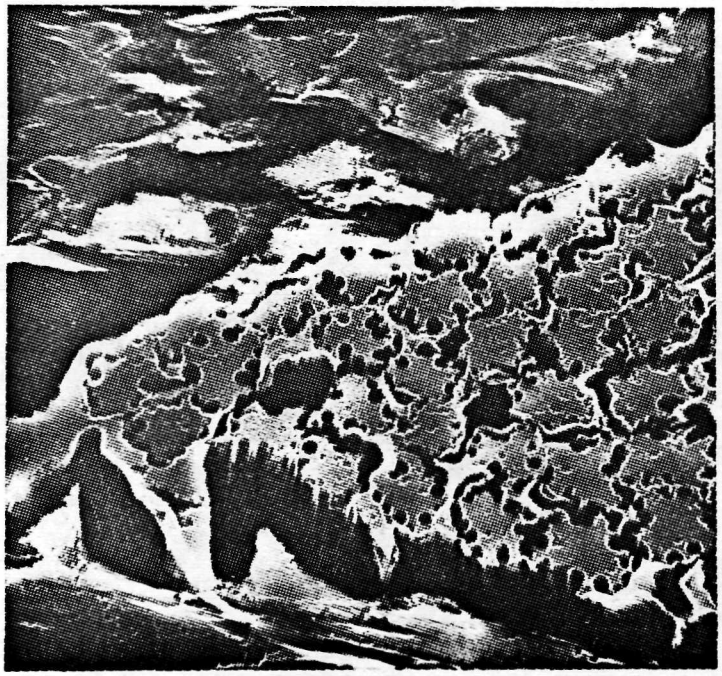

c) 12% burnoff, 1130x.

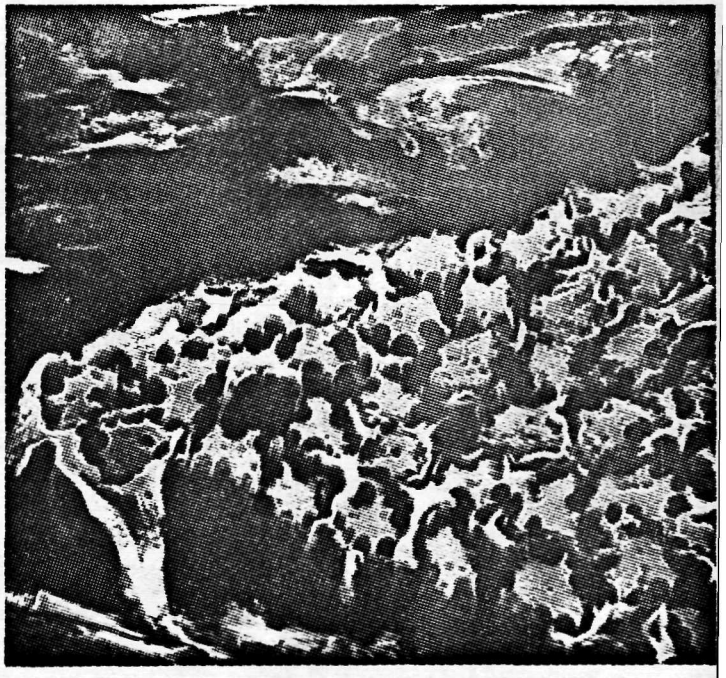

d) 15% burnoff, 1158x.

Figure 9. C-100 polished section (center of Fig. 8).

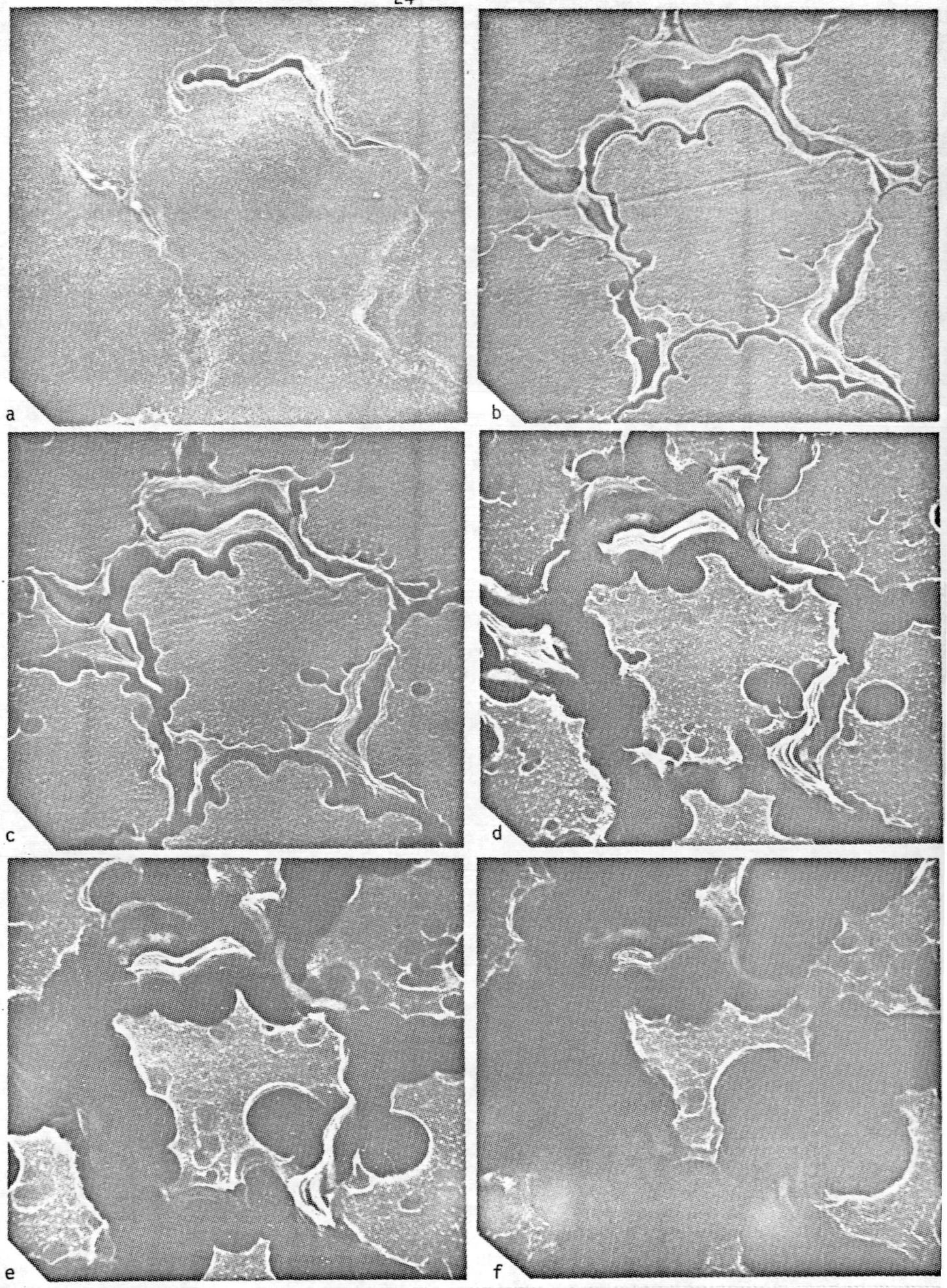

Figure 10. C-100 polished section oxidation sequence. a) 0% burnoff, 5300x; b) 2%, 5400x; c) 4%, 5270x; d) 12%, 5560x; e) 15%, 5625x; f) 20%, 5540x.

deep when they appear and grow radially. Adherent binder films (i.e. lower right side of the central fiber) do not appear to influence the heterogeneous attack, although they do seem to inhibit the more uniform general oxidation of the fiber lateral surfaces. Very fine light-toned particulate matter which appears on the fiber cross section after extensive oxidation (d,e,f) appears to be a residual ash from oxidized impurities (but a residue of alumina polishing grit cannot be ruled out on these polished surfaces). The inter-fiber binder films definitely become thinner as the oxidation proceeds, but it is not clear whether burnoff or "fall off", as the supporting fiber surfaces recede, is the principal binder loss mechanism. In any case, the residue remaining after very extensive burnoff consists primarily of fiber cores which seem to be less reactive than the original fiber surfaces.

The oxidation of a polished longitudinal section of a fiber is shown in Fig. 11 a,b,c,d. This section corresponds to a chord above the fiber axis (the section width is only about 5 μm, compared with the 8-10 μm fiber diameter, and the width increases as burnoff proceeds). The twin grooves at right center appear to be preparation artifacts, but could possibly be bottoms of crennulation grooves. The attack again initiates at pits on the lateral surfaces and the pits are now semicircular, suggesting hemispherical pitting. With continued burnoff these pits increase in diameter, binder disappears revealing more fiber width, and it appears that the pits may be located along a crennulation groove. Again, fine white particulate "ash" develops, especially along the pit rims, as oxidation progresses. The initial surface groove, whatever its nature, is not a preferential attack site. The attack which appears in the lower right corner of (c) apparently results from breakthru of a hemispherical pit which initiated below the polished surface plane.

Some observations on a C-100 cleavage surface are shown in Fig. 12 and 13. In Fig. 12 a (unoxidized) several "bare" fibers are revealed, surrounded by partially ruptured binder films. After the initial oxidation several flakes of binder have disappeared, evidently by falloff since there is little evidence of significant binder attack until later in the sequence. At higher magnification (not shown) a fine pitting attack can be seen, randomly distributed over the fiber surface. As the oxidization procedes, these fiber surface pits grow and are visible in (c); but aside from loss of some small loosely-attached fragments, little change is detectable in the binder phase. Finally, when only the central cores of the fibers remain (d), definite evidence of binder pitting and burnoff is seen. At high magnification (not shown) the sharp edges of the oxidized fiber cores are found to be decorated with fine, bright particles which are almost certainly ash since no polishing materials were used in preparing the cleavage surface. Figure 13 shows a single fractured fiber end, enclosed in a partially detached thin film of binder. The initial oxidation (b) produces pitting on the exposed fiber surface as well as some destruction of the binder film. It was observed that such films, when intact and adherent to the fiber surface, afforded some protection against attack to the fiber. In this figure, definite evidence of oxidation-deepening of the surface grooves, evident on the fractured cross section, is particularly

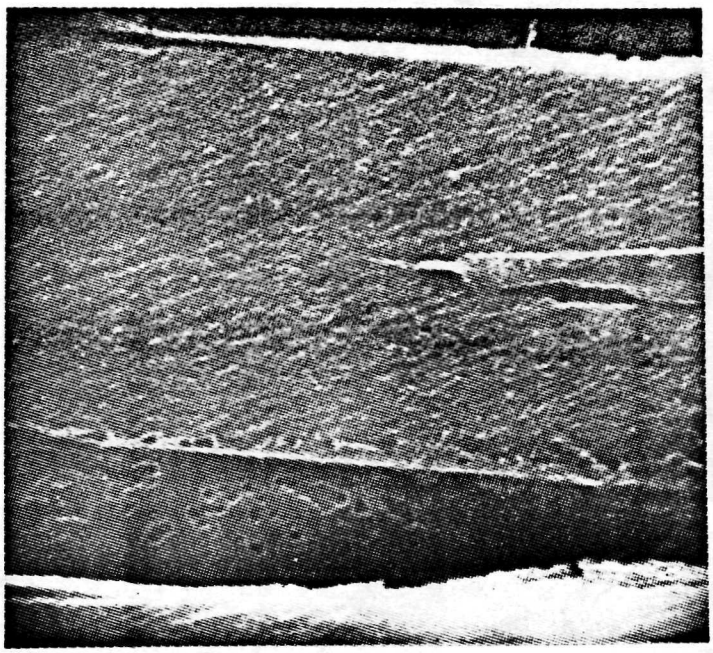

a) 2% burnoff, 11,100x.

b) 4% burnoff, 10,800x.

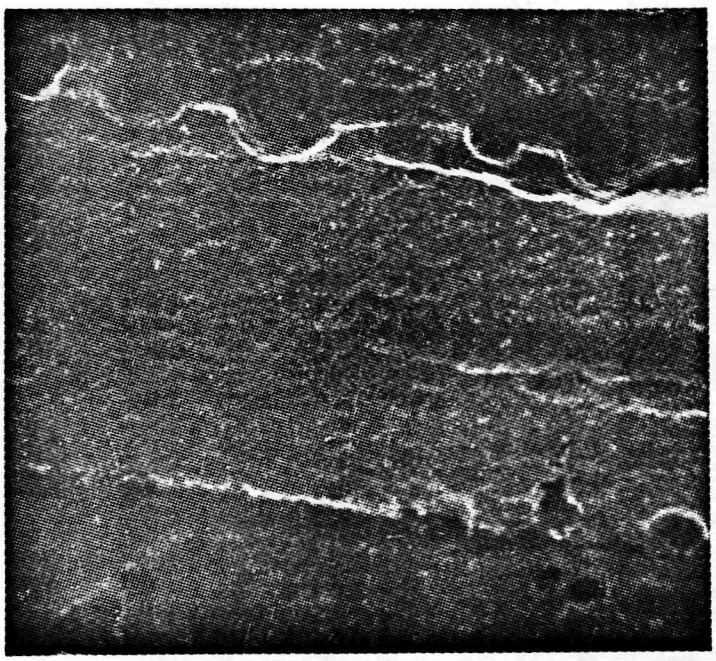

c) 10% burnoff, 11,150x.

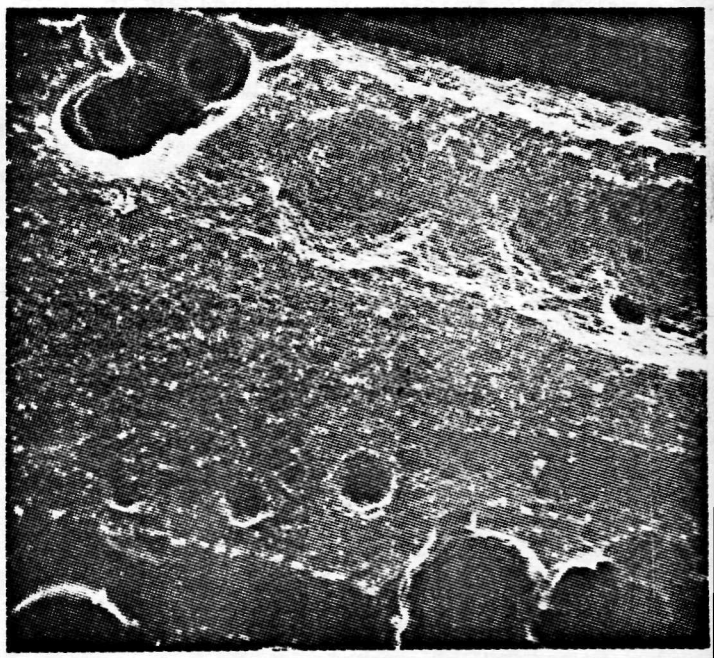

d) 15% burnoff, 11,600x.

Figure 11. Oxidation of C-100 polished section (different area).

a) 0% burnoff, 1040x.

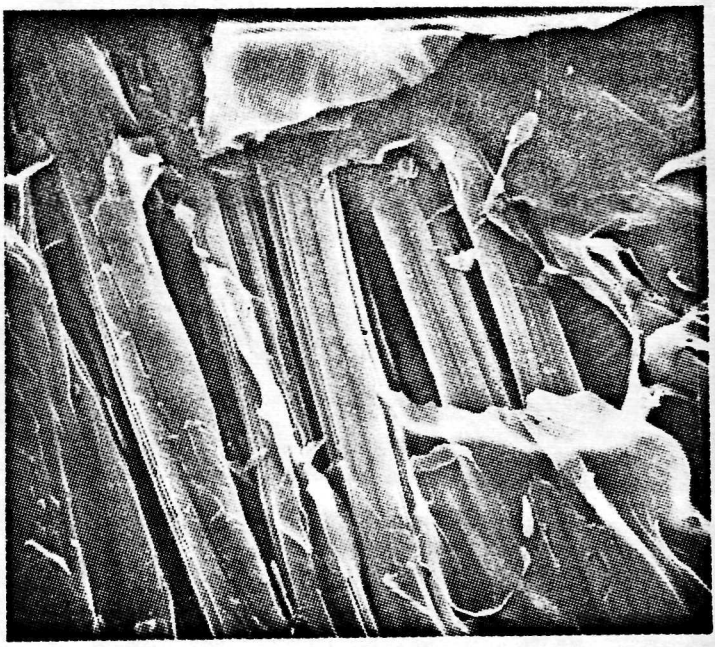

b) 1% burnoff, 1060x.

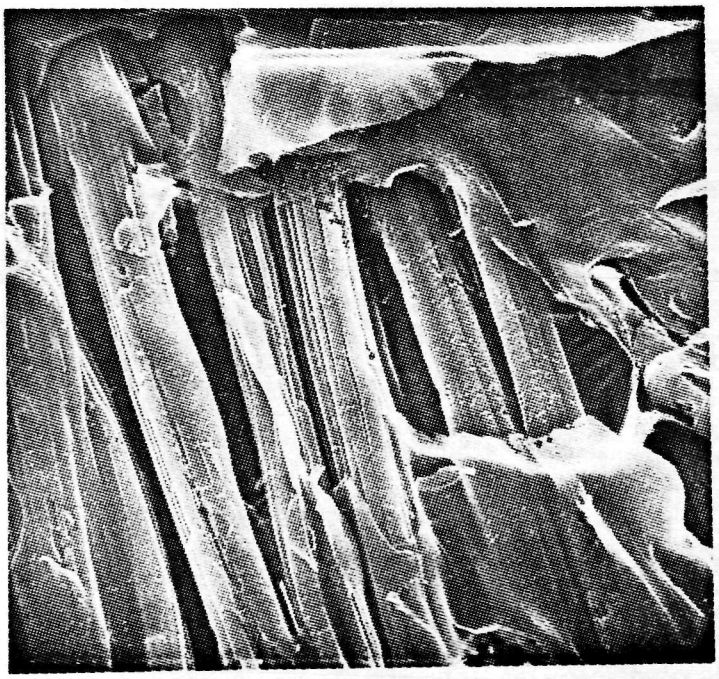

c) 2% burnoff, 1040x.

d) 4% burnoff, 1042x. (inverted)

Figure 12. Oxidation of C-100 cleavage.

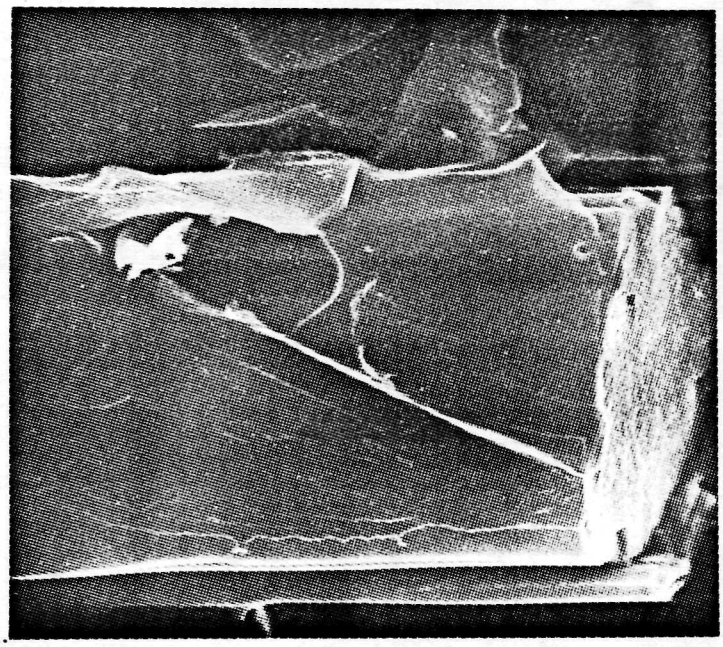

a) 0% burnoff, 5200x.

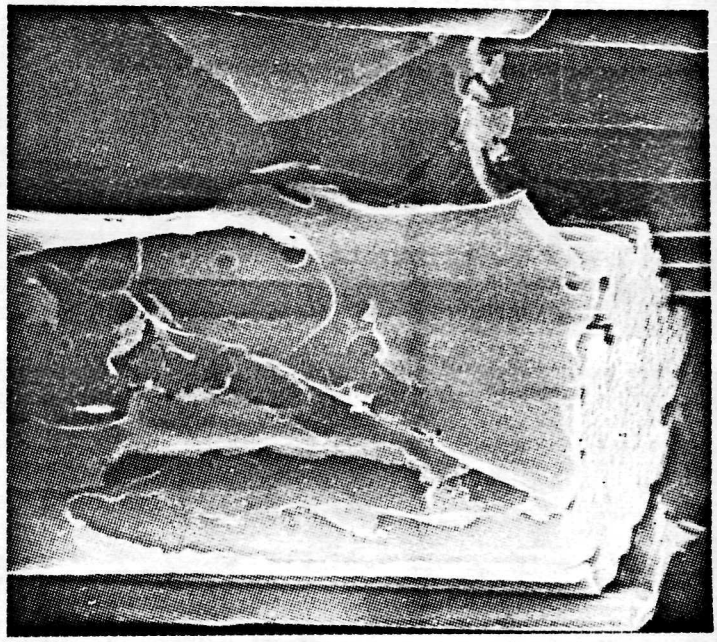

b) 2% burnoff, 5200x.

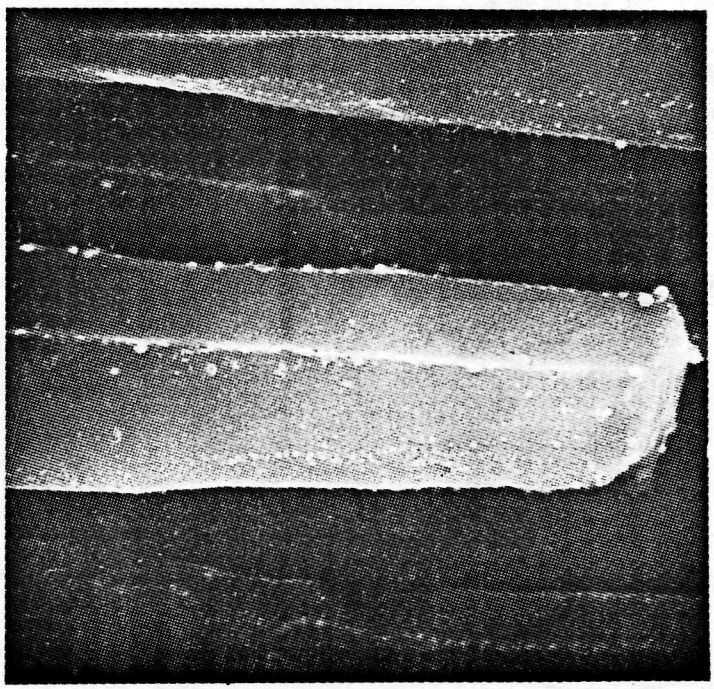

c) 4% burnoff, 5220x.

Figure 13. Single fiber detail, C-100 cleavage oxidation.

significant. A small flaw just beneath the base of a groove near the top of the fiber in (a) has opened up to join the groove in (b), and the other grooves also appear to have become deeper. Little if any uniform diameter decrease or recession of the fiber end surface has occurred, however. After extensive burnoff (c) a smooth surface, sharp-cornered fiber core remains, decorated along and near the edges with roughly spherical ash particles. The rapidity of the attack on the local region shown in Figs. 11, 12 relative to the total sample weight loss is notable and illustrates the difficulty of quantitatively relating micrographs to the burnoff curves of Fig. 6.

Summarizing the observations on C-100, porosity occurs at weave interstices (large diameter pores), at boundaries between plys, yarns and layers and within yarns (medium diameter) and at fiber/binder interfaces and within interfiber binder films (small pores). Both a laminar primary and an isotropic impregnant binder phase are present. Initial oxidation attack occurs preferentially on the lateral surfaces of the fibers, especially along or just beneath the bottoms of the longitudinal crennulation grooves, and deep circular holes appear and grow in these locations on polished fiber cross sections. Binder oxidation begins after the initial fiber attack, and then proceeds fairly rapidly. The binder offers some protection to the fiber surfaces, which are more reactive. After extensive burnoff the residue consists of fragments of the binder network and fiber cores. These fiber cores, which are evidently much less reactive than the outer fiber surfaces, often have smooth, sharp-edged lateral surfaces decorated with ash particles.

As might be anticipated, both the structure and the oxidation behavior of C-500 is generally similar to that of C-100. However, there are some significant differences associated with the use of graphitized fibers. Examination of polished cross sections reveals porosity that is much like that shown in Fig. 8a. The appearance after extensive oxidation, Fig. 14,

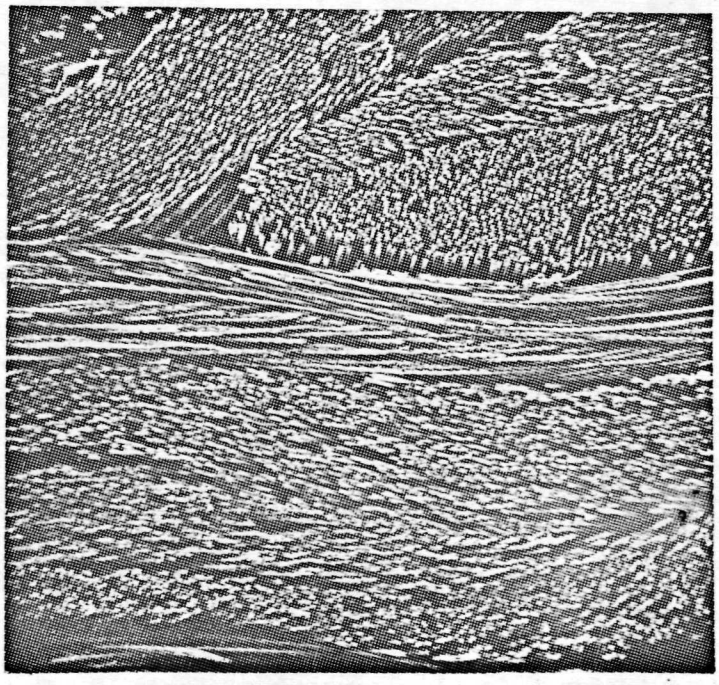

Figure 14. Polished cross section of C-500 after 15% burnoff. 113X.

gives the very strong impression that the residue consists of binder-free fibers. A high magnification oxidation sequence within a normally-sectioned yarn appears in Fig. 15 a,b,c,d,e,f. Note that this sequence begins with an oxidation-etched surface (about 1% sample weight loss). The small bright particles clearly visible on the fiber surfaces in (a) and (b) are primarily alumina polishing grit. Both the laminar primary binder and an apparently more isotropic and less reactive impregnant binder phase are clearly evident in (a) thru (d). Note that much of the impregnant binder is still present in (e) although the primary binder has completely disappeared. Both uniform lateral and deep-hole peripheral attack occurs on the fibers, similar to C-100. Moreover, spots which appear to be possible precursors of the deep-hole sites are faintly visible in (a) and details of the attack sequence can be followed in (b) and (c). Unfortunately, these sites were not recognized until the sequence was completed and no additional information was obtained on them. In comparison with C-100 (Fig. 10), attack on the polished fiber cross sections seems relatively more important, and the reactivity of the carbonized binder appears to equal or exceed that of the graphitized fibers. After about 15% burnoff only fiber cores remain with no trace of binder in this field of view. And there is nothing in this sequence to suggest that the binder offers any significant protection to the fibers. A longitudinally sectioned and polished yarn is shown in Fig. 16 a,b,c. The sequence begins after about 2% burnoff. There is evidence here of poor wetting and adherence between the binder and the fibers. The apparent particulate second phase within the binder is probably sectioned rods of impregnant binder intruded into cylindrical pores. As oxidation proceeds the binder phase is attacked first, but after appreciable burnoff a heavy pitting attack has occurred on the fibers as well. Intermediate pictures in this series (not shown) suggest that the attack on the fibers shows less preference for the lateral surfaces than in C-100.

The cleavage behavior of C-500 differs significantly from that of C-100 (and C-700). Cleaved surfaces consist mainly of bare, often broken fibers with little binder evident, as illustrated in Fig. 17. This effect is not entirely understood but it appears to result primarily from poor bonding between the graphitized fibers and the carbonized binder. A similar influence of fiber graphitization treatment on composite interfacial characteristics has been observed in studies on model uniaxial composites [10]. The oxidation of these bare fibers is often very heterogeneous, consisting of a localized deep pitting attack as shown here. A similar type of attack was observed in some regions of oxidized bare GSGC-2 cloth, as reported earlier [3]. This may result from localized impurity concentrations (or defective structures) which remain in the fibers after the graphitization treatment. Although the attack on the binder phase here is less intense than the localized fiber attack, binder reactivity appears to be comparable to or greater than the average fiber reactivity.

In summary, although the general microstructure of C-500 is very similar to that of C-100, close examination of polished cross sections as well as the general appearance of cleavage surfaces indicates that graphitization of the fiber phase has resulted in poor bonding with the carbonized binder

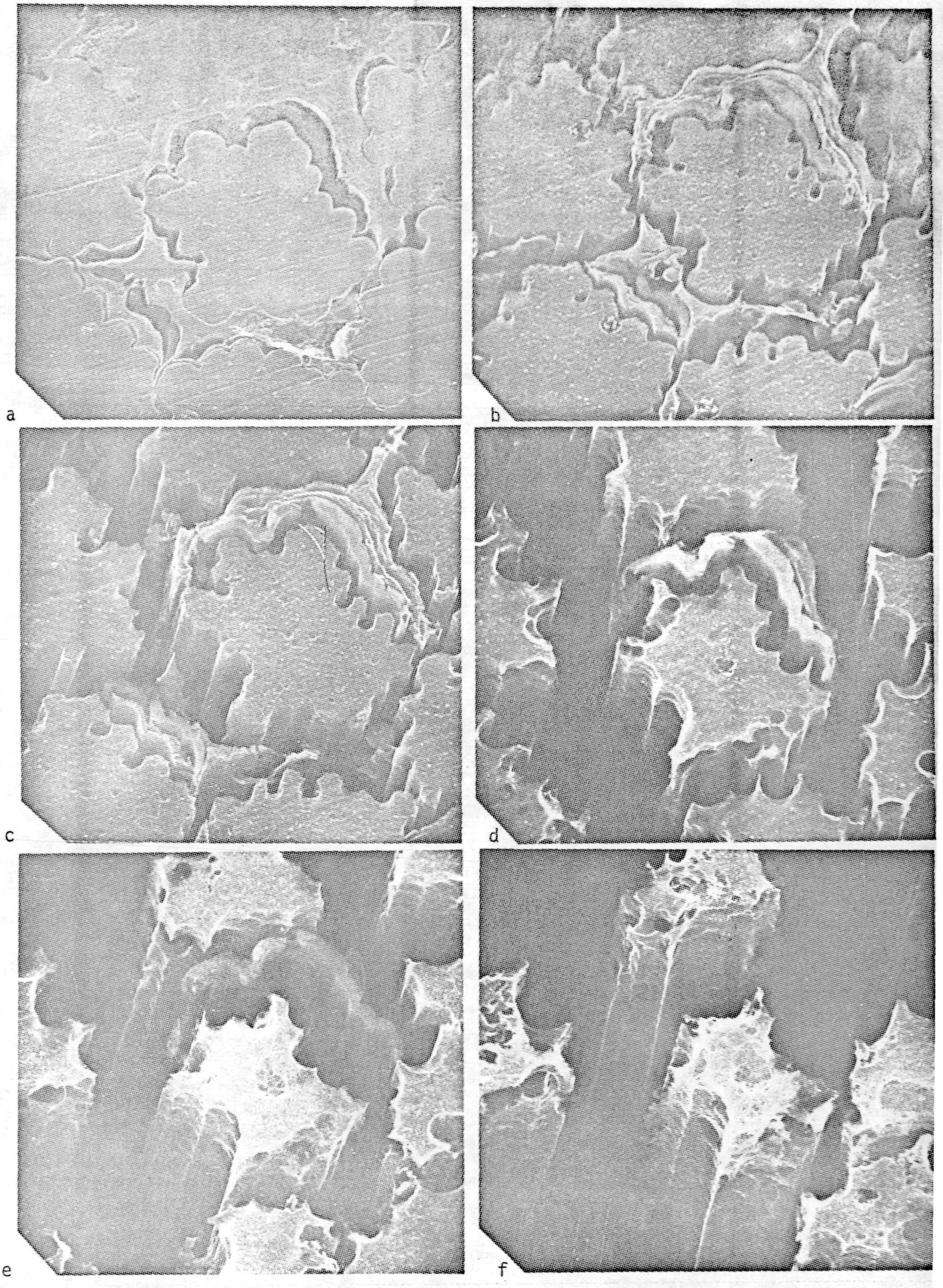

Figure 15. C-500 polished section oxidation sequence. a) 1% burnoff, 5360x; b) 4%, 5280x; c) 7.5%, 5650x; d) 10%, 5790x; e) 12%, 5580x; f) 15%, 5590x.

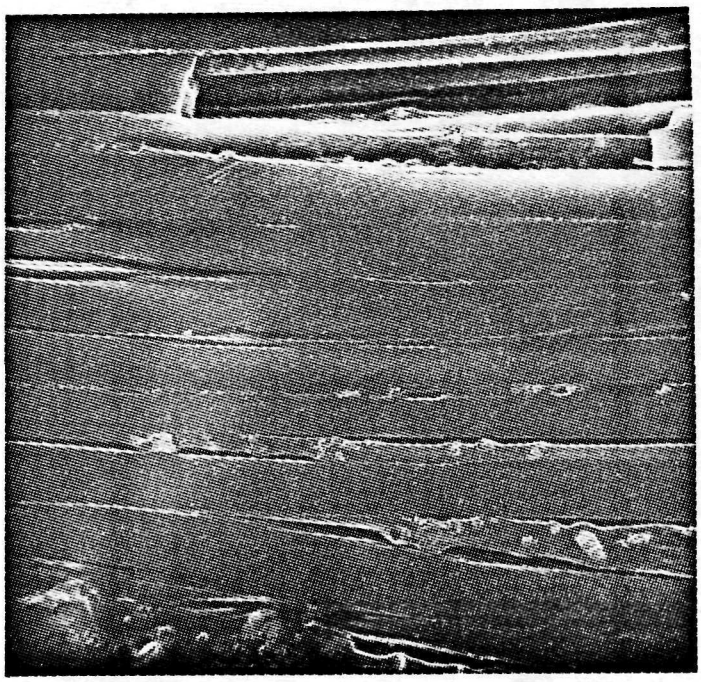

a) 2% burnoff, 1120x.

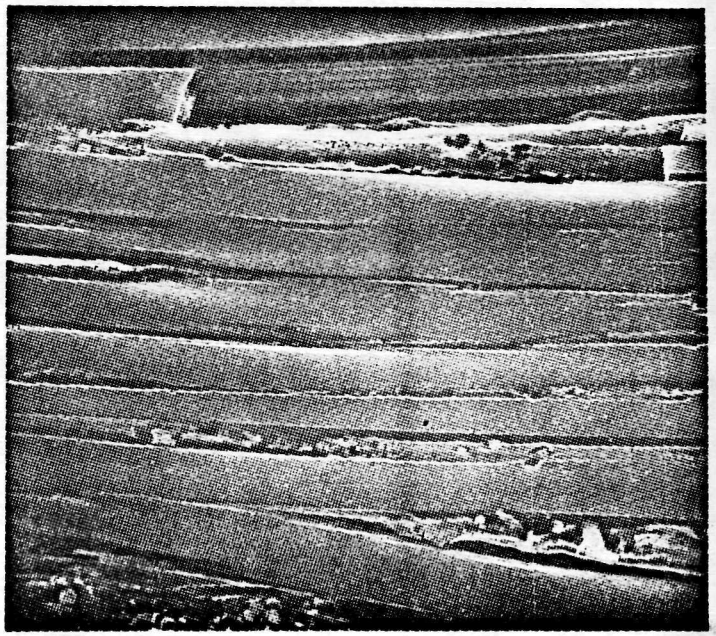

b) 7.5% burnoff, 1130x.

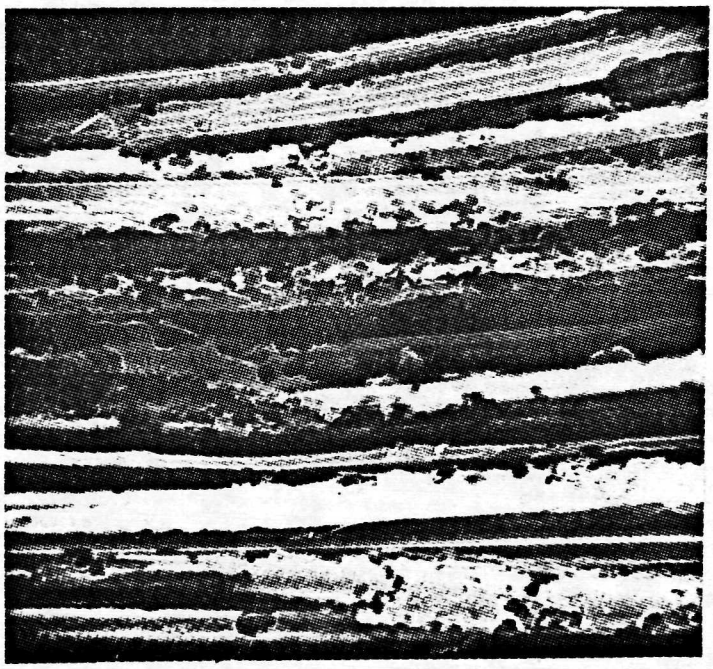

c) 15% burnoff, 1120x.

Figure 16. Oxidation of longitudinally-sectioned yarn, C-500 polished section.

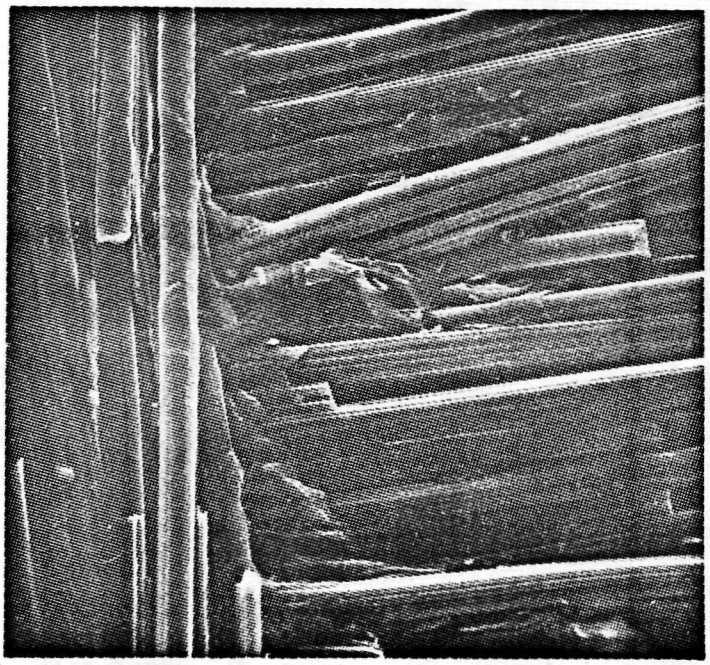

a) 0% burnoff, 552x.

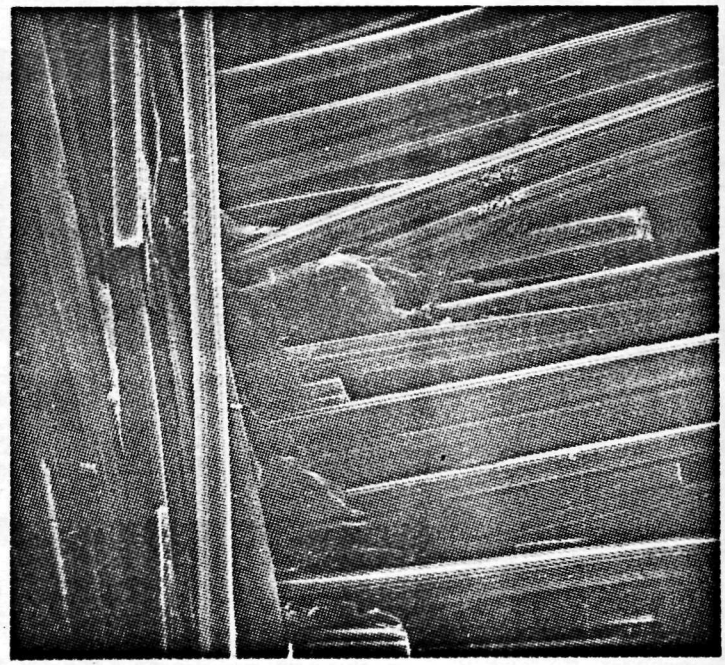

b) 4% burnoff, 560x.

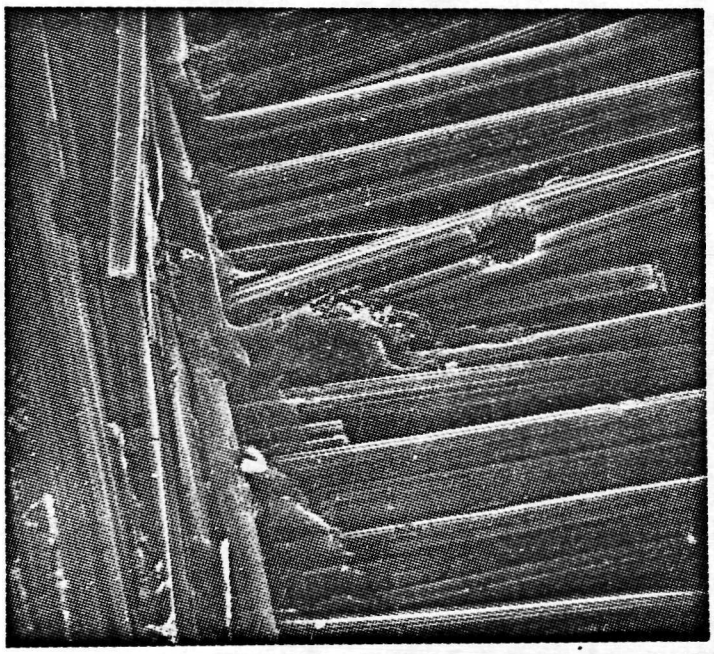

c) 7.5% burnoff, 558x.

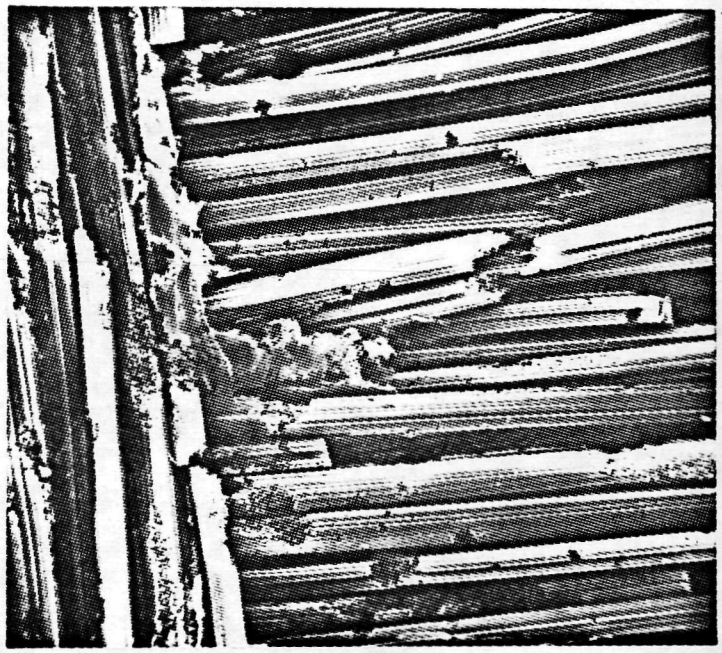

d) 10% burnoff, 588x.

Figure 17. Oxidation of C-500 cleavage.

matrix. Fine interfacial separations resulting from this condition may contribute to the very-small-diameter porosity detected in this material. The average reactivity of the binder phase appears to be comparable to or greater than that of the fibers, but a very rapid heterogeneous attack occurs at occasional active sites along the fiber length. After extensive burnoff, a residue of pitted fiber cores remains, with no clear or general evidence of significant ash. It appears that the lower burnoff rate of C-500 relative to that of C-100 may be attributed largely to reduction of fiber reactivity by the graphitization treatment.

C-700 is constructed from the same plain-weave cloth as C-100, 500 and the general appearance of cleavage and polished cross sections is similar to that shown in Fig. 7 (C-700, 730 pictures appeared in [1,2]). As judged from the cleavage behavior, graphitization of the composite evidently greatly improves the fiber/binder interactions relative to that observed in C-500. This effect is not understood (perhaps C-700 730 were fabricated from ungraphitized cloth after all). C-730 is constructed from a different (satin-type) cloth weave, resulting in a much flatter cleavage and a different cross sectional morphology as shown in Fig. 18 ab. Although the increased macroscopic anisotropy of C-730 has some influence on mechanical properties [1,2] it appears to have very little effect on the detailed microstructure or the oxidation behavior and a combined discussion of the two grades is given here. The oxidation-etched (1%) polished cross section, shown at moderate magnification in Fig. 19a, contains a distribution of porosity rather similar to that of the other grades (note that the magnification is twice that of Fig. 8). After appreciable oxidation, Fig. 19b, the structure remains quite compact without the large inter-yarn gaps evident in Figs. 8b and 14, and appears to consist of fiber cores in a recessed but still present binder matrix. The progressive attack on a polished cross section is shown at high magnification in Fig. 20 a,b,c,d. The as-polished view (a) is unusually clear here and the small separations between fiber and binder which probably contribute the 0.4 μm pore mode are evident. After an average burnoff of only 1% these gaps are much wider and much more prevalent. Measurements made on these pictures indicate that the gaps grow primarily by reduction in fiber diameter, but thinning of the binder webs also occurs. The primary (lighter-toned) binder is not only laminar by "polygonized" (kinked and segmented) as a result of the graphitization. There is a suggestion of a poorly developed laminar structure in the graphitized impregnant binder (darker tone) as well, and it seems to be a little less reactive than the primary binder. An adherent primary binder film seems to protect the lower right side of the central fiber from attack thru the entire sequence though it is progressively attenuated in thickness and undercut by oxidation from the end. Oxidation of the fibers is similar to that in C-500, though there is little evidence here of precursor sites for the deep-hole attack. In the initial oxidation studies on these materials [2] regions of the polished surface were observed where a catastrophic preferential attack on the fibers had occurred early in the burnoff sequence, leaving behind an empty honeycomb matrix of binder. We were not able to reproduce this behavior and it is not clear whether it was a peculiarity of the particular samples tested or of the technique used. In at least one early experiment, a bit of conductive silver paint (used to attach the samples to mounting stubs for SEM studies) got onto the

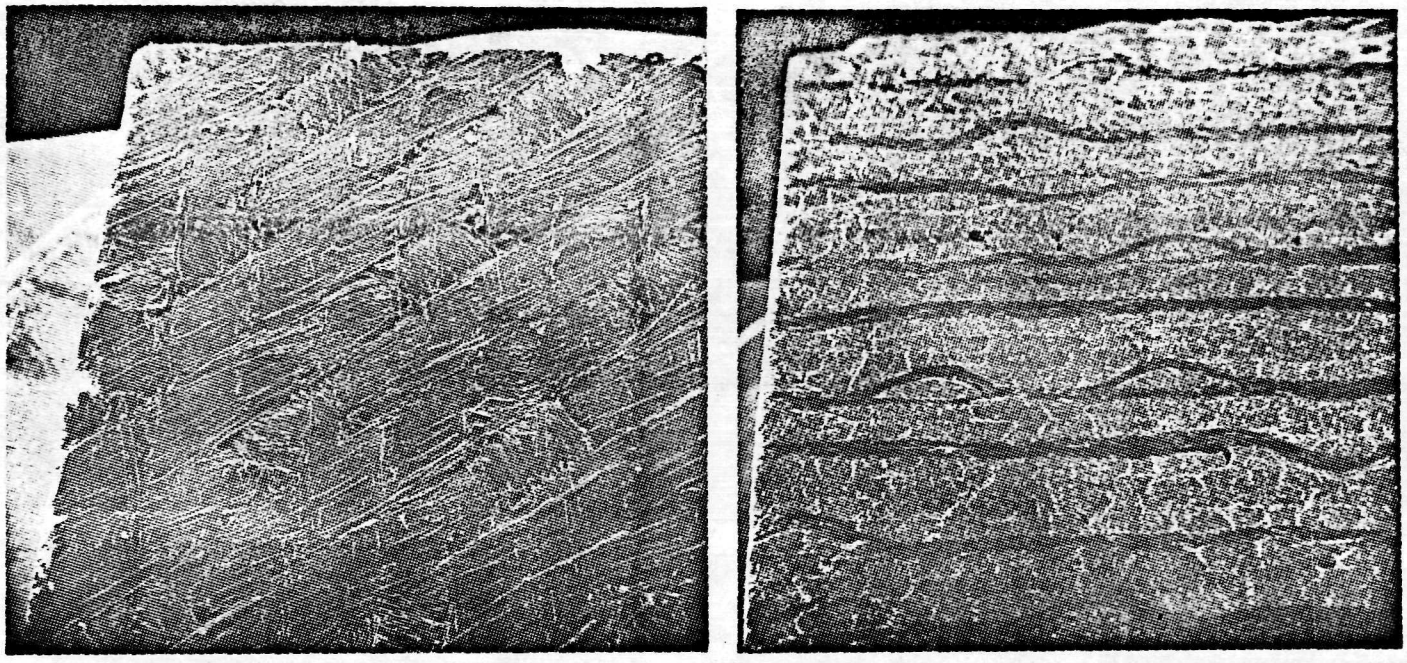

a) Cleavage, 0% burnoff, 21x. b) Polished section, 5% burnoff, 22x.

Figure 18. Macrostructure of Carbitex 730.

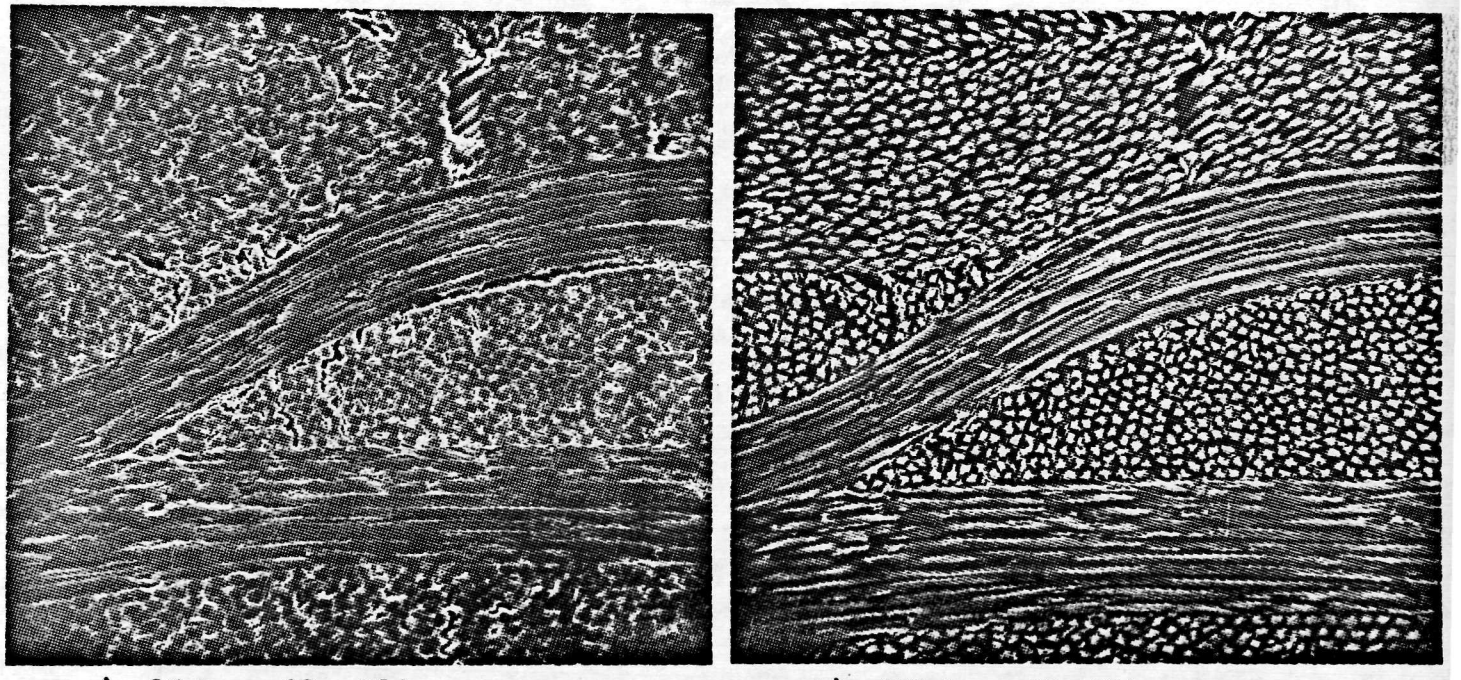

a) 1% burnoff, 214x. b) 15% burnoff, 224x.

Figure 19. Detail of C-730 polished section (center of Fig. 18b).

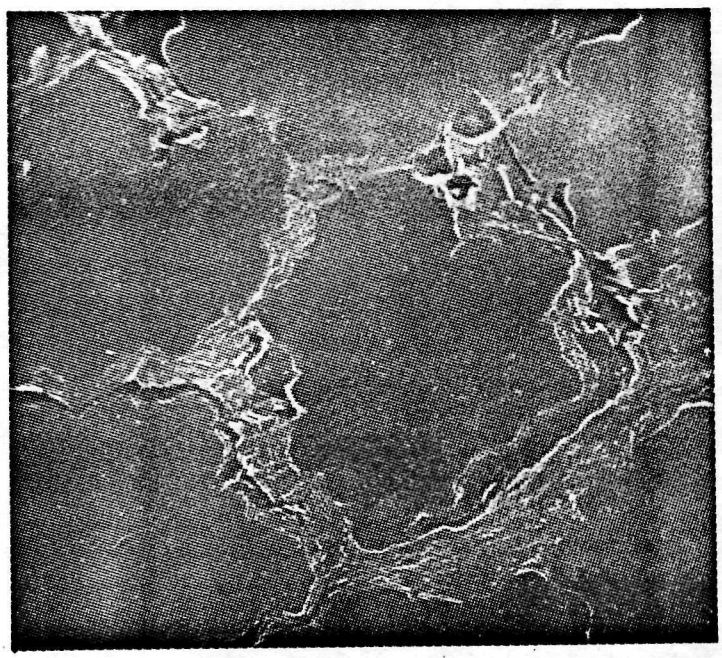

a) 0% burnoff, 5470x.

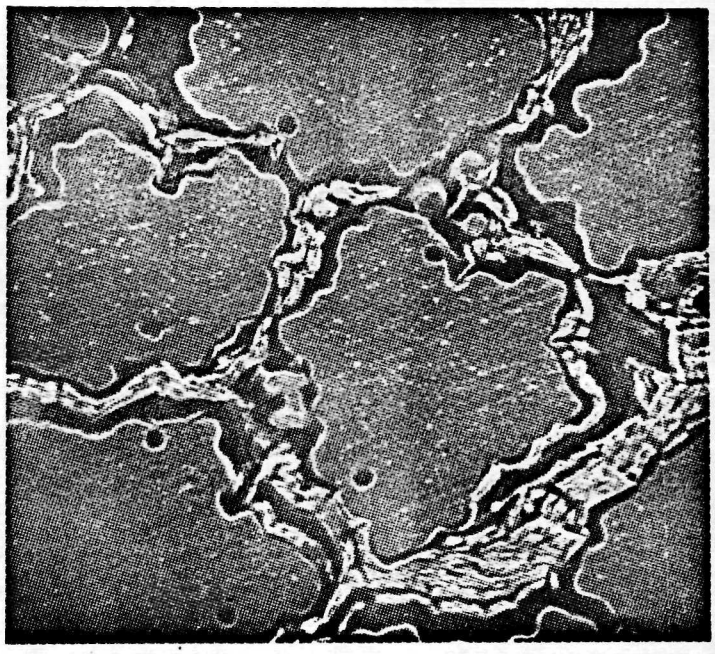

b) 1% burnoff, 5300x.

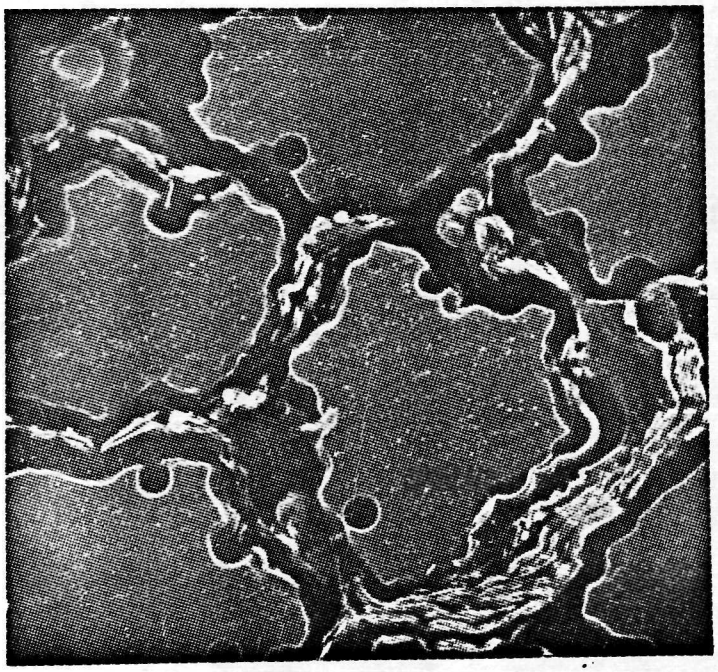

c) 4% burnoff, 5215x.

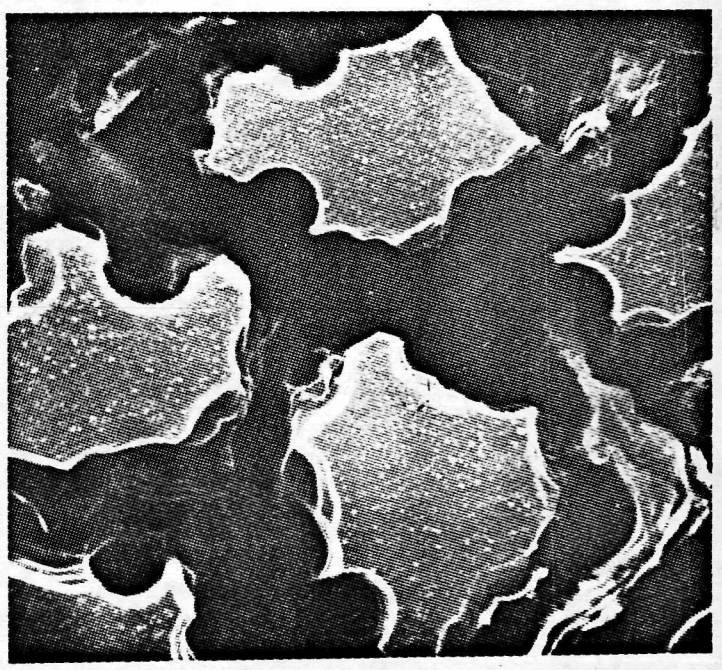

d) 10% burnoff, 5630x.

Figure 20. Oxidation sequence on C-730 polished section.

observed surface and catalyzed a severe local attack during the subsequent oxidation treatment. Thereafter, great care was taken to ensure that the samples were free of such foreign material when they were oxidized.

In general, the binder phase in these graphitized composites appears to be significantly less reactive than the fiber phase. Figure 21 shows a typical cleavage surface. It is composed primarily of an interlaminar

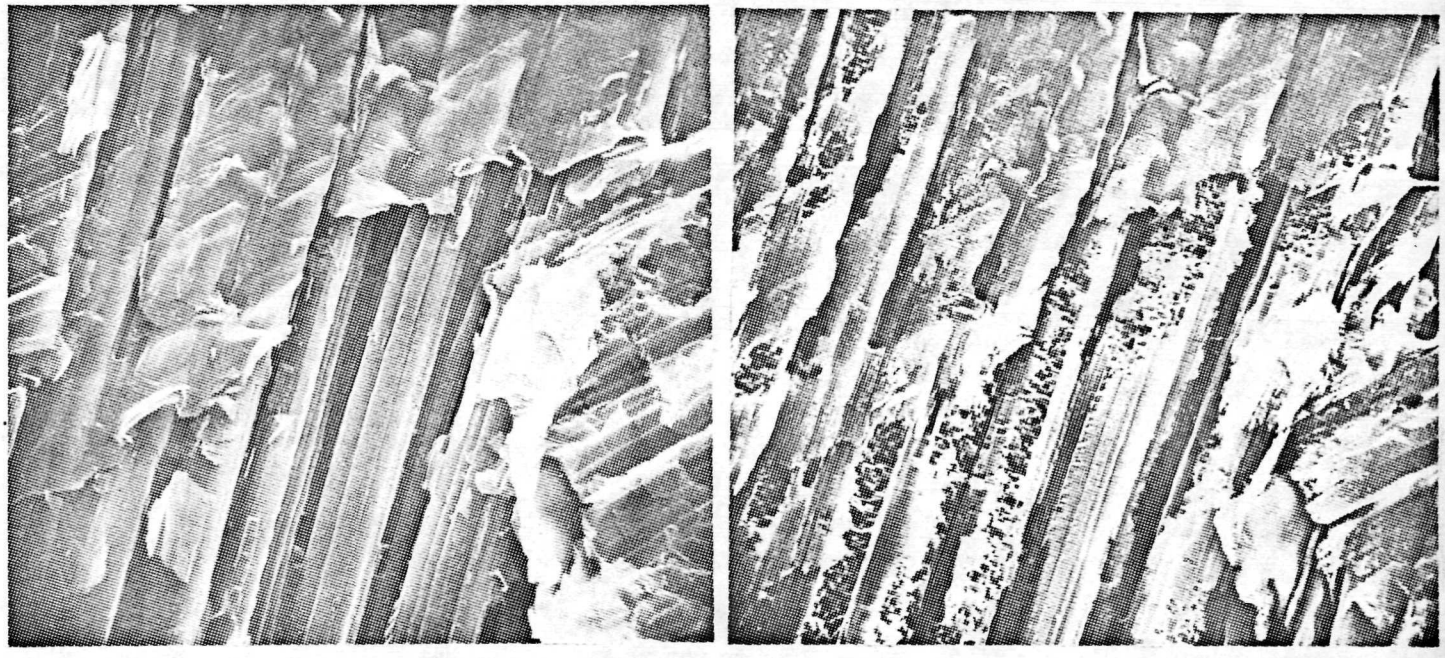

Figure 21. Cleavage surface of C-700: a) Unoxidized, 1095X; b) 13% burnoff; 1068X

binder film bearing diagonal imprints of the fibers in the mating surface; and in the center of the picture, fibers from which the binder layer has been stripped. After a burnoff of about 13% much of the binder remains, but the exposed fibers have been heavily though heterogeneously attacked. Although not clearly evident at this magnification, the unoxidized fiber (lower center) is protected by a thin film of binder. A portion of this central fiber and the development of oxidation attack upon it is shown in the high magnification sequence, Fig. 22 a,b,c,d. In Fig. 22a it can be seen that the fiber is coated with a thin, wrinkled skin of binder which is largely adherent and intact, but has been ruptured (probably during cleavage or handling) in several places at the upper left. The detailed origin of this skin is not known (e.g., a pre-preg coating on the cloth before fabrication of the composite; precipitation of mesophase from a thermoplastic primary binder, etc.). In any case evidence of similar thin binder films were observed in both C-100 (Fig. 13) and C-500 where they were unwrinkled but poorly adherent and not particularly effective in influencing fiber oxidation. The appearance here is consistent with the presence of a highly oriented film (layer planes parallel to the fiber surfaces) which conformed closely to the fiber at the graphitization temperature. However, the thermal

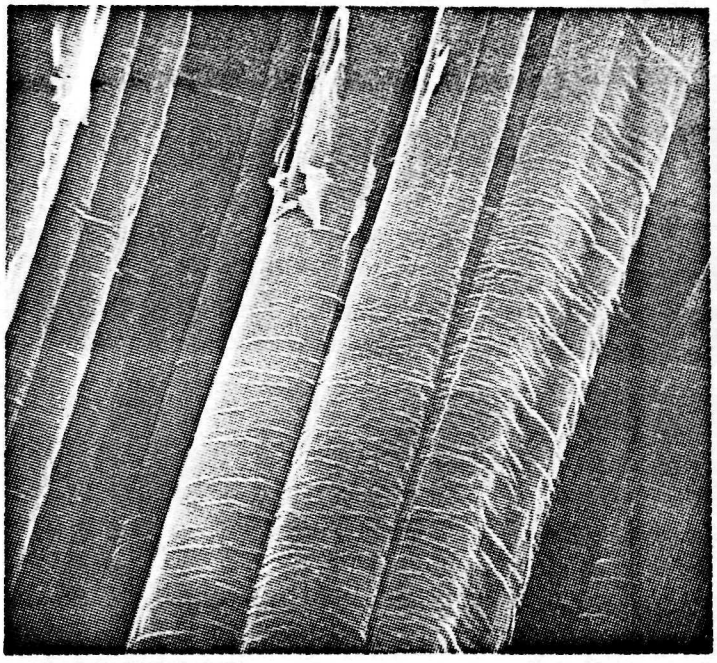

a) 0% burnoff, 5460x.

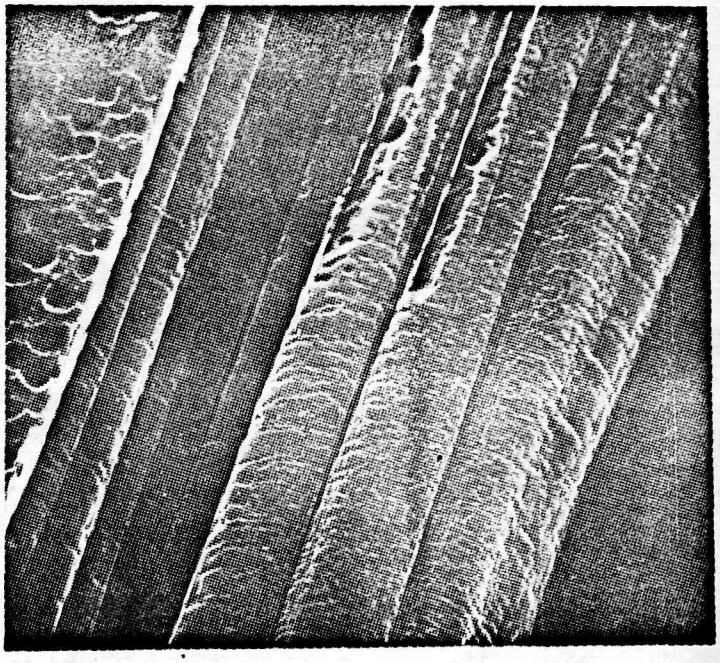

b) 4% burnoff, 5080x.

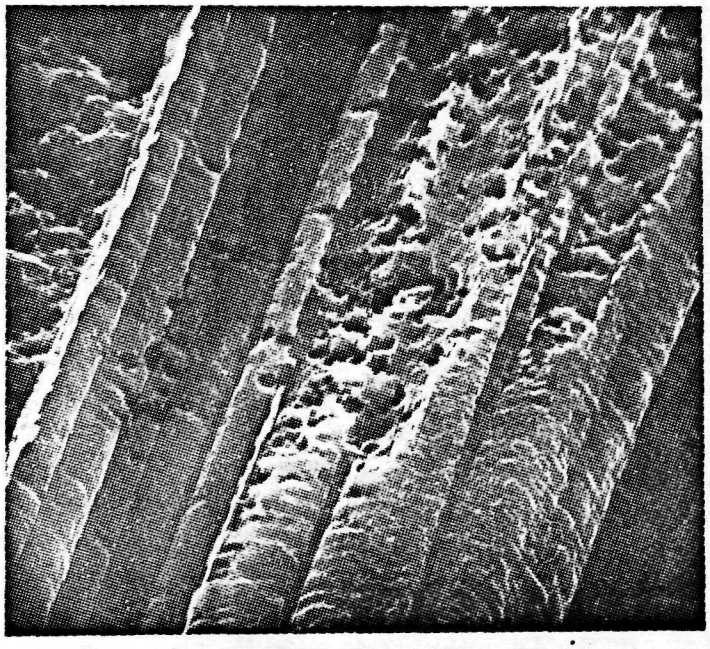

c) 8.5% burnoff, 5370x.

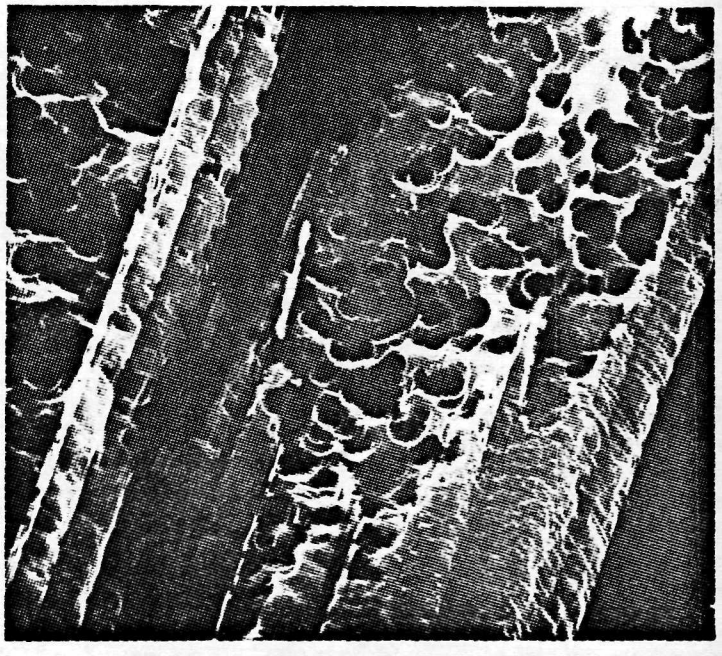

d) 13% burnoff, 5380x.

Figure 22. Detail of C-700 cleavage oxidation (center of Fig. 21).

expansion coefficient of the low orientation-texture fiber is greater than that of the oriented binder (especially in the longitudinal direction), and on cool down from the processing temperature the film is stressed in compression causing it to deform by kinking and to separate locally from the fiber, though the film remains intact. Attack begins where the binder film is ruptured (Fig. 22b) and spreads progressively along the fiber (c,d), apparently undermining and dislodging the film. After 13% burnoff, Fig. 22d (and even after 20%, not shown) the lower right portion of the fiber which is still coated with binder has not yet been significantly oxidized, though the rest of the fiber has been largely consumed and the binder film also shows definite evidence of oxidation.

In summary, the microstructural differences associated with the satin-type cloth weave in C-730 have little influence on the burnoff process. C-700 and C-730 are very similar in their oxidation behavior and differ significantly from the C-100, 500 materials primarily because of graphitization of the binder phases. Again, two binder phases are present but graphitization has caused polygonization of the laminar primary binder, the development of a suggestion of laminar structure in the secondary binder, and an apparently significant improvement in binder/fiber bonding over that observed in C-500. One aspect of this improvement is the occurrence of thin, wrinkled but adherent binder films coating the individual fibers. Oxidation attack on the fiber phase is similar to that observed in C-500, but the graphitized binder phase is significantly less reactive, and the binder skin on the fibers, when intact, is quite effective in protecting them from attack. Even at very high burnoff levels there is little change in the macroscopic size and appearance of C-700,730. It appears that a residual network of unconsumed binder is largely responsible for this behavior, though fiber cores certainly remain as well, and earlier observations of rapid preferential fiber attack leaving an empty honeycomb web of binder residue could not be reproduced. These observations suggest that a more effective impregnation with graphitized binder and/or sealing of exposed surfaces with graphite (or a CVD carbon deposit) could further reduce the oxidation rate of these composites toward that of the pyrolytic and glassy carbons.

Conclusions:

Characterization of the microstructures and investigation of the oxidation behavior of Carbitex 100 (carbon fibers in carbonized binder), 500 (graphitized fibers in carbonized binder) and 700, 730 (graphitized fibers and binder, two different cloth weaves) yielded the following conclusions:

1. X-ray diffraction spectra do not resolve the separate binder and fiber phases. The binder phase appears to be generally more graphitic than the fibers and to dominate the lattice parameter values, but in C-500 the fiber phase seems to determine the (001) peak shape. Mean interlayer spacing decreases (degree of graphitization increases) in the order GSCY-2-10 carbonized fiber (very disordered); C-100; GSGC-2,8 graphitized fibers; C-500; C-700; C-730 (quite well graphitized). The binder phase has a pronounced orientation texture (layer planes parallel to the fiber axes) in all the composites.

2. Bulk densities ranged from 1.327 (C-100) to 1.468 (C-730). Immersion densities (benzene/tetrabromoethane gradient column) ranged from 1.458 (carbonized fiber) and 1.474 (C-100) to 1.668 (C-700). Fractional pore volumes calculated from the density data increased in the order C-500 (7.4%), C-730 (8.8-9.7%), C-100 (10.1%), C-700 (12.3-13.5%). The flat satin-type weave evidently contributes to the lower C-730 porosity; a deficiency of binder contributes to the high porosity and low density of C-100; and graphitization treatment generates increased open porosity.

3. The porosity is distributed trimodally in the pore entrance-diameter range $D > 200$ A (a small additional fine-pore mode in the range $D < 200$ A was also indicated for C-500). The detailed distribution depends systematically on the fabrication and processing of the composite. Macropores ($D \geq 100$ μm) are attributed to incomplete binder penetration, especially of weave interstices. Small pores ($\bar{D} \simeq 0.45$ μm) appear to be associated with separations at the binder/fiber interface and perhaps within the binder phase. The medium-sized pore mode ($2.5 \leq \bar{D} \leq 7$ m), attributed to gaps between yarns or plys, is particularly sensitive to cloth weave and thermal processing history. Mercury porosimetry at high pressures causes irreversible structural damage, perhaps compaction of the composite.

4. SEM observations on both cleavage and polished cross section surfaces generally confirmed the structural inferences drawn above. In addition, they revealed the presence of at least two binder phases: A laminar primary binder which is polygonalized by graphitization, and a more isotropic-appearing impregnant binder. Cleavage appearance showed that fiber/binder bonding in C-500 is poor compared to that in C-100 or C-700, 730. Thin adherent binder films wrinkled by differential thermal compaction stresses coat the fibers in C-700, 730; unwrinkled, poorly adherent films of binder occur on the fibers in C-100, and perhaps C-500.

5. Macroscopic burnoff rates in dry air at 650°C are about an order of magnitude faster for C-100, 500 than for C-700, 730 (which are about ten times faster than pyrolytic or glassy carbon according to 550°C ambient air results). C-100 oxidizes a little faster than C-500; and C-700 a bit faster than C-730. These small differences correlate with relative porosity but other factors are involved as well. Rates increase with increasing burnoff, probably due to increasing accessible surface area. The large difference in reactivity between the carbonized and the graphitized composites must be attributed primarily to the influence of thermal treatment on structural disorder and impurity content.

6. Microscopically, for comparable thermal histories, fiber lateral surfaces oxidize more readily than the binder. Lateral surfaces of the fibers are attacked first, especially at the bottoms of longitudinal surface grooves, breaking thru as deep circular holes on polished cross sections. Fiber cores, which are less reactive, remain after extensive burnoff. They are decorated with ash residue in C-100. For bare graphitized

fibers (C-500, GSGC cloth) a heterogeneous attack occurs at active sites distributed along the fiber lengths. In C-700, 730 an adherent coating of binder inhibits attack on the fibers; and a similar but less pronounced effect seems to occur in C-100. Relative reactivities appear to be as follows: In general, primary binder > impregnant binder; fiber lateral surfaces > fiber core, fiber cross section, or binder; on the average for high burnoff, binder $\sim$ fiber in C-100; binder > fiber in C-500; binder < fiber in C-700, 730.

7. Oxidation resistance of composites is improved by a) graphitization, b) adherent graphitized coatings, especially on fibers, c) high density. For short-time exposures, surface sealing with graphitized or carbonized binder, or a pyrolytic (CVD) carbon coating might be effective in further decreasing reactivity.

Acknowledgements:

It is a pleasure to thank T. Radly, A. Ramming and J. E. McKean of the Carborundum Company for providing gratis samples of the Carbitex materials; C. S. Kucheria for assistance with the porosimetry studies; A. Miller and M. Rorabaugh for assistance in taking the x-ray diffraction data; and NASA Research Grant #NGL 48-002-004, "Interdisciplinary Research Concerning the Nature and Properties of Ceramic Materials", for major support of the Principal Investigator on this grant.

References:

1. D. B. Fischbach and David Uptegrove, "Structural Studies on Carbon Materials for Aerospace Refractory Applications" Semi-Annual Report #1 (for period 15 Sept. '71 - 15 Mar. '72), NASA Research Grant #NGR 48-002-129. May 1972.

2. D. B. Fischbach and David Uptegrove, Semi-Annual Progress Rept #2 (for period 16 Mar. - 15 Sept. '72). 27 Dec. 1972.

3. D. B. Fischbach, D. Uptegrove and S. Srinivasagopalan, "Structural Studies on Carbon Materials for Advanced Space Technology" Semi-Annual Progress Report #3 (for period 16 Sept. '72 - 15 Mar. '73). NASA Grant #NGR 48-002-129, Supplement #1, 1 May 1973.

4. S. Srinivasagopalan and D. B. Fischbach, "Indentation Microhardness Behavior of Some Homogeneous Carbon Materials", Bulletin Amer. Cer. Soc. 59 (9), Sept. 1973 (Abstract of paper presented at Pacific Coast Regional Meeting of ACS, San Francisco, 30 Oct. - 2 Nov. 1973).

5. D. R. Uptegrove and D. B. Fischbach, "SEM Observations on Oxidation Behavior of Some Carbon/Carbon Composites" ibid.

6. D. B. Fischbach and C. S. Kucheria, "Porosity of Some Laminar Carbon/Carbon Composites" extended abstract submitted for presentation at 4th London International Carbon-Graphite Conference, 23-27 Sept. 1974.

7. C. W. Rohl and J. H. Robinson, "Fiber Reinforced Carbon and Graphite" Research/Development, July 1966. Also Carborundum Company Bulleting #112, "Carborundum Carbitex" 1965.

8. J. D. Brooks and G. H. Taylor, "The Formation of Some Graphitizing Carbons" in Chemistry and Physics of Carbon, P. L. Walker, Jr., editor, Dekker, New York 1968, Vol. 4, pp. 243-86.

9. R. D. Reiswig, L. S. Levinson and J. A. O'Rourke, "Graphitization of Polyfurfuryl Alcohol" Carbon 6 (1), 124 (L), Feb. 1968.

10. E. Fitzer and B. Terwiesch, "Carbon/Carbon Composites Unidirectionally Reinforced with Carbon and Graphite Fibers" Carbon 10 (4), 383-90, Aug. 1972.

11. D. H. T. Specner, "The use of Molecular Probes in the Characterization of Carbonaceous Material", in Porous Solids, R. L. Bond, editor, Academic Press, New York, 1967, pp. 87-154.

12. J. M. Dickinson and J. W. Shore, "Observations Concerning the Determination of Porosities in Graphite" Carbon 6 (6) 937, Dec. 1968.

13. D. Baylink, J. Sipe, J. Wergedal and O. J. Whittemore, "Vitamin D Enhanced Osteocytic and Osteoclastic Bone Resorption" Amer. J. Physiology 224 (6) 1345-57, June 1973.

14. D. J. Baker and J. B. Morris, "Structural Damage in Graphite Occurring During Pore Size Measurements by High Pressure Mercury" Carbon 9 (5) 687-90, Oct. 1971.

15. J. B. Lewis, "Thermal Gas Reactions of Graphite" in Modern Aspects of Graphite Technology, L. G. F. Blackman, editor, Academic Press, New York, 1970, pp. 129-199.

16. Maurice Letort, "Introduction a l'etude de la vitesse et du mecanisme de combustion des carbones", (and following sections) in Les Carbones Vol. II, by Le Groupe Francais d'etude des Carbones, Masson and Cie, Paris, 1965.